Isoform-specific nicotinic responses are present in distinct subtypes of prefrontal layer V pyramidal neurons

Ashutosh V. Patel[1,3], Anthony Nguyen[1], Pietro Paletta[2], Elena Choleris[2] and Craig D.C. Bailey[1]*

[1]Department of Biomedical Sciences, University of Guelph, Guelph, ON, Canada. [2]Department of Psychology, University of Guelph, Guelph, ON, Canada. [3]Present address: Department of Psychology, University of Toronto Scarborough, Toronto, ON, Canada.

*email: baileyc@uoguelph.ca

Abstract

The neurotransmitter acetylcholine supports goal-directed cognitive functions via activation of its nicotinic and muscarinic classes of receptors within the prefrontal cortex. These receptors are expressed on pyramidal neurons located within layer V of the prefrontal cortex, which integrate afferent signals and contribute toward cognitive circuits via efferent projections to cortical and subcortical targets. Using whole-cell electrophysiology, retrograde labelling, and neuron reconstruction in the juvenile mouse prefrontal cortex, we identified three unique isoform-specific nicotinic receptor responses that are present in distinct subtypes of layer V pyramidal neurons. Broadly, we observed α7 or α7/β2* nicotinic responses in burst-firing neurons that project to the contralateral cortex or nucleus accumbens, respectively, and β2* nicotinic responses in regular-firing neurons that project to the ventromedial thalamus. These findings provide insight into a receptor isoform-specific mechanism by which nicotinic acetylcholine neurotransmission may support cognitive functions via modulation of distinct efferent projections from this brain region.

Introduction

The modulatory neurotransmitter acetylcholine (ACh) acts within the rodent medial prefrontal cortex (mPFC) to support goal-directed cognitive functions such as working memory and attention[1-3]. The manner by which ACh fulfills this role is sophisticated and likely multimodal[4,5], as evidence exists for both a sustained tonic increase in extracellular ACh content[6,7] and a transient phasic increase in synaptic ACh content[1,2] for animals performing visual attention tasks. ACh activation of its nicotinic class of receptor (nAChR) plays an important role in this process. For example, the pharmacological or genetic disruption of nAChR function impairs performance[3,8-12] and the pharmacological augmentation of nAChR function enhances performance[12-14] for mPFC-dependent tests of cognitive function. The nAChR comprises a group of pentameric ligand-gated ion channels that are permeable to monovalent and divalent cations. The two predominant nAChR isoforms within the mPFC are homomeric α7 nAChRs (composed of five α7 subunits) and heteromeric β2* nAChRs (composed of α4 and β2 subunits with the potential incorporation of one α5 subunit). These isoforms possess distinct functional properties and are differentially expressed within cellular layers and neuron types of the mPFC (reviewed in Abbondanza and colleagues[15]). Within layer V of the mPFC, it has been observed that pyramidal neurons express α7 nAChRs and that both fast-spiking and non-fast spiking interneurons may express combinations of α7 and/or β2* nAChRs[16,17]. However, evidence suggests that layer V pyramidal neurons within other cortical regions express both α7 and β2* nAChRs[18]. It is important to determine whether layer V pyramidal neurons within the mPFC also express both receptor isoforms because this will further our understanding of the sophisticated manner by which cholinergic neurotransmission supports mPFC-based cognitive circuits and behaviours.

Layer V pyramidal neurons integrate inputs from cortical and subcortical sources, placing them in an important position to contribute toward cognitive circuits. They are a

heterogeneous population based on electrophysiological and morphological properties. Previous research over the past four decades has characterized layer V pyramidal neurons in multiple cortical regions, allowing for the discovery of distinct neuron subtypes having specific action potential firing patterns, apical dendrite morphologies, and axonal projection targets. In response to depolarizing current injection, action potential firing patterns are described as intrinsically burst-firing (BF) or regular-firing (RF), with sub-variations being reported within each of these categories[19-34]. Although precise terminology can vary depending on the study, BF neurons commonly are described as exhibiting true all-or-nothing bursts of action potentials[19-21,26,33], or two-to-four action potentials with a markedly short interspike interval (ISI) at the beginning of a train of action potentials[22-25,29,30,32]. RF neurons exhibit a relatively longer, sometimes adapting ISI throughout a train of action potentials[19-30,32]. Other properties of BF and RF neurons are often found to distinguish them into groups having distinct apical dendrite morphologies and axonal projections. In sensory and motor cortices, BF neurons typically have “wide” or “thick” apical dendrite tufts and are “pyramidal tract” (PT) neurons that project to subcortical regions including the striatum, thalamus, spinal cord, pons, and superior colliculus whereas RF neurons typically have “narrow” or “thin” apical dendrite tufts and are “intratelencephalic” (IT) neurons that project to the contralateral cortex and striatum[20,23,25,30,33,35-41]. These properties do not align perfectly in all reports, suggesting potential variation based on sex, age, or recording conditions[23,24,37,42,43]. Moreover, properties of these broad neuron subtypes may differ between sensorimotor and associative cortical regions[34]. In the mPFC, combinations of BF trains, IT/striatal projections, and narrow/thin apical dendrite tufts are typically observed while combinations of RF trains, PT projections, and wide/thick apical dendrite tufts are typically observed[32,34,44,45], although this is not always found for all properties[31,32] and both BF and RF neurons have been identified in PT and IT populations in unspecified frontal cortex[27,28]

83 In this present study, we identify and characterize unique isoform-specific nicotinic
84 responses in three distinct pyramidal neuron subtypes within mPFC layer V sampled from
85 juvenile mice of each sex. Like previous work in mPFC described above, each of these neuron
86 subtypes has its own combination of action potential firing pattern, apical dendrite morphology,
87 and projection target(s). Specifically, we show that α7 nAChR responses are present in BF
88 neurons that have narrow (male) or wide (female) apical dendrite tufts and project to the
89 contralateral mPFC, a combination of α7 and β2* nAChR responses are present in BF neurons
90 that have wide (male) or narrow (female) apical dendrite tufts and project to the ipsilateral
91 ventral striatum (nucleus accumbens), and β2* nAChR responses are present in RF neurons
92 that have wide (male) or narrow (female) apical dendrite tufts and project to the ipsilateral
93 ventromedial thalamus. This work adds the dimension of nicotinic response type and sex
94 differences to the known properties of mPFC layer V pyramidal neuron subtypes, and provides
95 insight into an nAChR isoform-specific mechanism by which cholinergic neurotransmission may
96 influence efferent signalling from this brain region.

97 **Results**

98 **Three unique nicotinic responses are present in mPFC layer V pyramidal neuron**
99 **subtypes.** Pyramidal neurons within layer V of the mPFC may be categorized into two broad
100 subtypes based on their action potential firing patterns in response to depolarizing current
101 injection. Under our recording conditions in juvenile mice, the injection of 200 pA depolarizing
102 current from rest for 500 ms identified a subtype of BF neurons based on a short initial ISI
103 between the first two action potentials of <10 ms and a subtype of RF neurons based on a
104 relatively longer ISI between the first two action potentials of >10 ms (Fig. 1). The BF subtype
105 may be further divided based on the nicotinic response types that were observed. Pressure
106 application of 1 mM ACh for 100 ms elicited one of two nicotinic responses in BF neurons,
107 which had either a fast rise and fast decay (Fig. $1a_2$) or a fast rise and two-phase fast plus slow
108 decay (Fig. $1b_2$). Responses with a fast rise and fast decay were not affected by the β2* nAChR
109 antagonist dihydro-β-erythroidine (DHβE) but were inhibited completely by the α7 nAChR
110 antagonist methyllycaconitine (MLA) (Fig. 1a), which is consistent with previous reports that α7
111 nAChRs are present on cortical layer V pyramidal neurons[16,18]. Responses with a fast rise and
112 two-phase decay had fast components inhibited by MLA and the remaining slow components
113 inhibited by DHβE (Fig. 1b), suggesting the presence of both α7 and β2* nAChRs, and possibly
114 also the presence of α7β2 heteromeric nAChRs containing both α7 and β2 subunits (reviewed
115 by Wu and colleagues[46]; referred to herein as α7/β2* responses). We did not test for the
116 presence of true α7β2 heteromeric nAChRs in these neurons because the subunit-selective
117 antagonists MLA and DHβE also inhibit this receptor isoform[47,48]. This same ACh application to
118 RF neurons consistently elicited responses with a slow rise and slow decay that were
119 characteristic of β2* nAChRs[3,49]. This was confirmed pharmacologically, as these responses
120 were unaffected by MLA but were inhibited completely by DHβE (Fig. 1c). Contingency analysis
121 revealed that approximately half of recorded neurons were BF and modulated by α7 responses

122 only (male: 29/57; female: 35/63), approximately one-quarter of neurons are BF and modulated
123 by α7/β2* responses (male: 13/57; female: 15/63), and approximately one-quarter of neurons
124 are RF and modulated by β2* responses only (male: 15/57; female: 13/63) (Fig. 1d). These
125 distributions did not differ between sexes (Chi-square test, $p = 0.76$).

Figure 1

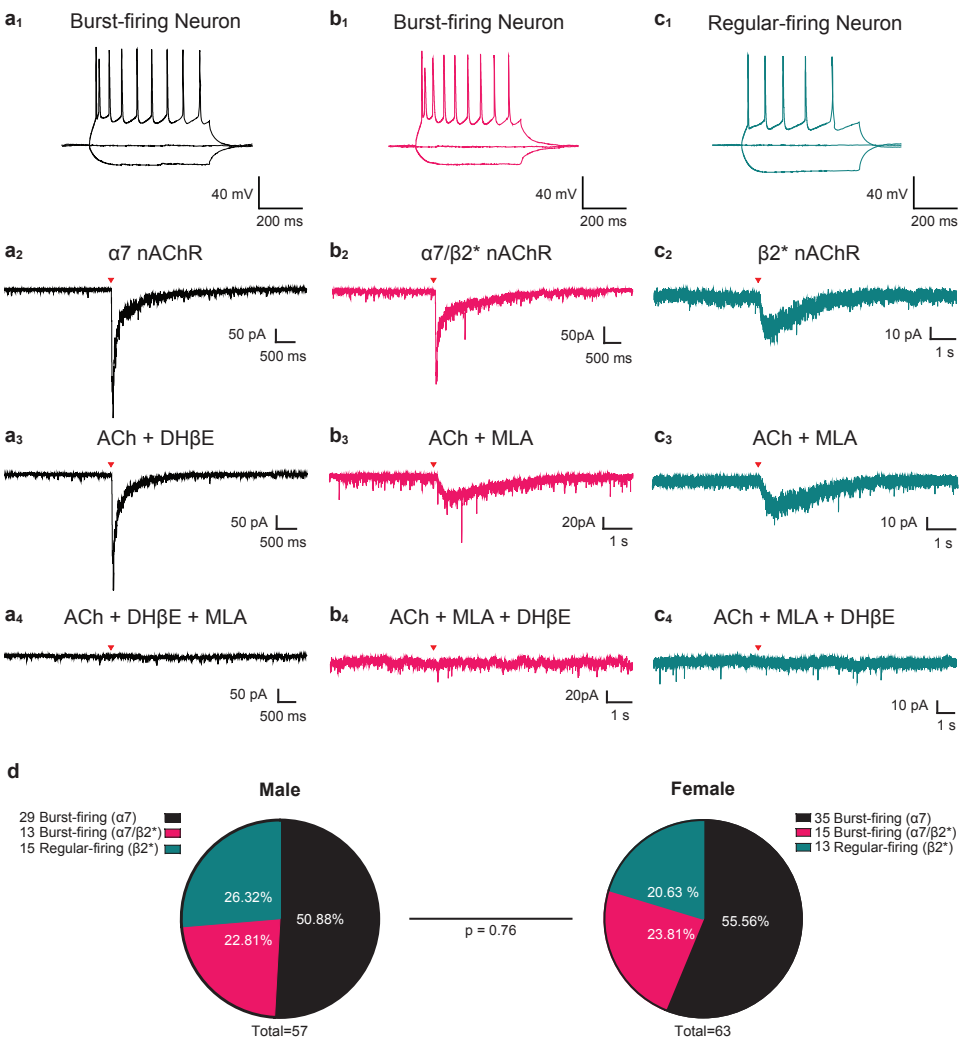

Fig. 1 Nicotinic responses observed in prefrontal layer V pyramidal neurons. Pyramidal neurons were sampled randomly from layer V of the juvenile mouse mPFC and recorded for intrinsic electrophysiological properties and nicotinic acetylcholine responses. Three unique nicotinic responses were observed within distinct neuron subtypes. **a** The most common nicotinic response was found in neurons that exhibited an initial burst-firing action potential firing pattern in response to the injection of 200 pA positive current (**a$_1$**). This nicotinic response to 100 ms application of 1 mM ACh (indicated by the red arrowhead in **a$_2$**) had fast rise and decay kinetics characteristic of homomeric α7 nAChRs, which was confirmed by the lack of effect of 3 μM DHβE (**a$_3$**) and the complete inhibition by 10 nM MLA (**a$_4$**). A second nicotinic response was also found in neurons that exhibited a burst-firing action potential firing pattern (**b$_1$**). Decay kinetics of this nicotinic response contained both fast and slow components (**b$_2$**). The fast component was inhibited by 10 nM MLA (**b$_3$**) and the remaining slow component was inhibited by 3 μM DHβE (**b$_4$**), which suggests the presence of both homomeric α7 and heteromeric β2* nAChRs. A third nicotinic response was found in neurons that exhibited a regular-firing action potential firing pattern (**c$_1$**). This nicotinic responses had slow rise and decay

142 kinetics characteristic of heteromeric β2* nAChRs (**c_2**). This was confirmed by the lack of effect
143 of 10 nM MLA (**c_3**) and the complete inhibition by 3 μM DHβE (**c_4**). **d** Pie charts show the
144 proportion of sampled neurons that exhibited each type of firing pattern and nicotinic response
145 for male and female mice. These proportions were not statistically different between sexes (Chi-
146 square test, X^2 (2, n = 120) = 0.55, p = 0.76).

147 Previous studies have characterized the kinetics of nicotinic responses mediated by α7,
148 α7β2 and β2* nAChRs[48,50]. We measured the kinetics of the three nAChR response types
149 observed in this study by fitting current responses to an eight-term Fourier series equation (Fig.
150 2). Current amplitude (Fig. 2a) differed amongst response types (two-way ANOVA, $F(2,112) =$
151 16.29, $p < 0.0001$) with α7 responses having a greater amplitude than α7/β2* and β2* responses
152 in males and β2* responses in females (Bonferroni *post hoc* correction, each $p < 0.01$). The net
153 charge (Fig. 2b) differed amongst response types ($F(2,114) = 64.61$, $p < 0.0001$) with the β2*
154 response having greater net charge than α7 and α7/β2* responses in both sexes (each $p <$
155 0.01). The time to the peak response (Fig. 2c) differed amongst response types ($F(2,114) =$
156 196.10, $p < 0.0001$ with the β2* response having a greater time to peak than α7 and α7/β2*
157 responses in both sexes (each $p < 0.0001$). Similarly, rise tau (Fig. 2d) differed amongst
158 response types ($F(2,114) = 84.42$, $p < 0.0001$ with the β2* response having a greater rise tau
159 than α7 and α7/β2* responses in both sexes (each $p < 0.0001$). The first decay tau (Fig. 2e)
160 differed amongst response types ($F(2,114) = 418.80$, $p < 0.0001$) with the β2* response having a
161 greater first decay tau than α7 and α7/β2* responses in both sexes (each $p < 0.0001$). This
162 measure also differed between α7 and α7/β2* responses in females only ($p < 0.01$). The second
163 decay tau (Fig. 2f) differed amongst response types ($F(2,114) = 361.60$, $p < 0.0001$) and reliably
164 differentiated the three response types, as each was different than the other in both sexes (each
165 $p < 0.0001$). This measure is particularly sensitive to differentiating α7 and α7/β2* responses, as
166 the second decay tau was less than 1000 ms for α7 responses and greater than 1000 ms for
167 α7/β2* responses. These analyses demonstrate that whole-cell α7, α7/β2*, and β2* nicotinic
168 responses have distinct activation and desensitization kinetics in juvenile mouse mPFC layer V
169 pyramidal neurons.

Figure 2

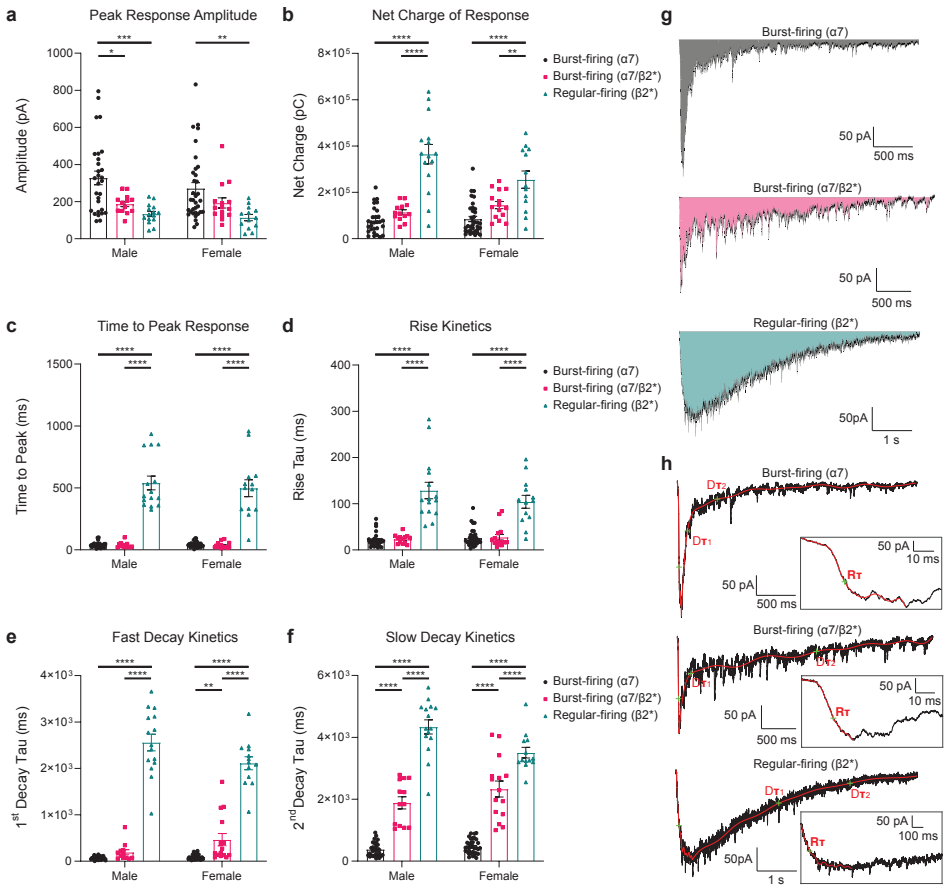

Fig. 2 Characterization of nicotinic responses in prefrontal layer V pyramidal neurons. A detailed analysis of inward current response kinetics was performed for the three pharmacologically-identified nicotinic responses that were observed within each neuron subtype. Peak response amplitude (**a**) and net charge (**b**) showed no sex difference (two-way ANOVA, each $p \geq 0.2$) but did show opposite effects of response type (each $p < 0.0001$). The time to peak (**c**) and rise tau (**d**) showed no sex difference (each $p \geq 0.4$), but were both affected by response type (each $p \leq 0.0001$) with β2* nAChR responses exhibiting the slowest response onset. The first decay tau (**e**) and second decay tau (**f**) showed no sex difference (each $p \geq 0.4$), but were both affected by response type (each $p \leq 0.0001$) with β2* nAChR responses exhibiting the slowest response decay amongst the response types. Of note, the second decay tau was significantly different between each the α7, α7/β2*, and β2* nAChR responses within each sex (Bonferroni *post hoc* correction, each comparison $p < 0.0001$). **g** One typical tracing is shown for each nicotinic response type with the solid area under the curve representing the net charge conducted. **h** The same typical tracings are shown with an eight-term Fourier series curve fitting to determine rise and decay kinetics. The rise tau (R_τ) is indicated by the green cross within each expanded box, while the first decay tau ($D_{\tau 1}$) and second decay tau ($D_{\tau 2}$) are indicated by green crosses within the full tracings. All data are shown for individual neurons and as mean +/- 1 SEM. Sample sizes for males are: burst-firing (α7) = 29; burst-firing (α7/β2*) = 13; regular-firing (β2*) = 15, and for females are: burst-firing

190 (α7) = 35; burst-firing (α7/β2*) = 15; regular-firing (β2*) = 13. Significance levels for Bonferroni
191 *post hoc* corrections within each sex are *$p < 0.05$, **$p < 0.01$, ***$p < 0.001$, and ****$p < 0.0001$.

192 **Intrinsic electrophysiological properties of layer V pyramidal neuron subtypes.** Having
193 categorized the recorded pyramidal neurons into three subtypes based on action potential firing
194 patterns and nicotinic response types, we next analyzed the intrinsic electrophysiological
195 properties of each neuron subtype (Fig. 3). Two-way ANOVA demonstrated that resting
196 membrane potential does not differ between neuron subtypes ($F(2,114) = 2.33$, $p = 0.1$) or
197 sexes ($F(1,114) = 0.25$, $p = 0.6$). Input resistance (Fig. 3a) was affected by neuron subtype
198 ($F(2,114) = 29.26$, $p < 0.0001$) with resistance being greater in RF (β2*) neurons than in each of
199 the BF subtypes (Bonferroni *post hoc* correction, each $p < 0.001$). As expected, ISI ratio (Fig.
200 3b) was affected by neuron subtype ($F(2,113) = 46.71$, $p < 0.0001$) with the ISI ratio being
201 greater in RF (β2*) neurons than in each of the BF subtypes (each $p < 0.001$). Rheobase (Fig
202 3c) showed an effect of neuron subtype ($F(2,113) = 5.10$), $p = 0.008$) although sag ratio (Fig 3d)
203 did not $F(2,114) = 2.67$, $p = 0.07$). Additional analyses revealed differences in active
204 electrophysiological properties between neuron subtypes. For example, within input/output
205 experiments RF (β2*) neurons exhibited greater excitability and a noticeable depolarization
206 block in both sexes (Fig. 3e-f). The magnitude of the post-firing afterhyperpolarization (AHP),
207 which influences excitability, also differed between neuron subtypes. In both sexes, there was a
208 significant interaction between the number of action potentials and AHP magnitude (Fig. 3g-h).
209 Overall, these analyses demonstrate that the passive and active intrinsic electrophysiological
210 properties differ between the layer V pyramidal neuron subtypes of this study, with the two BF
211 subtypes being similar to each other and different from the RF (β2*) subtype.

Figure 3

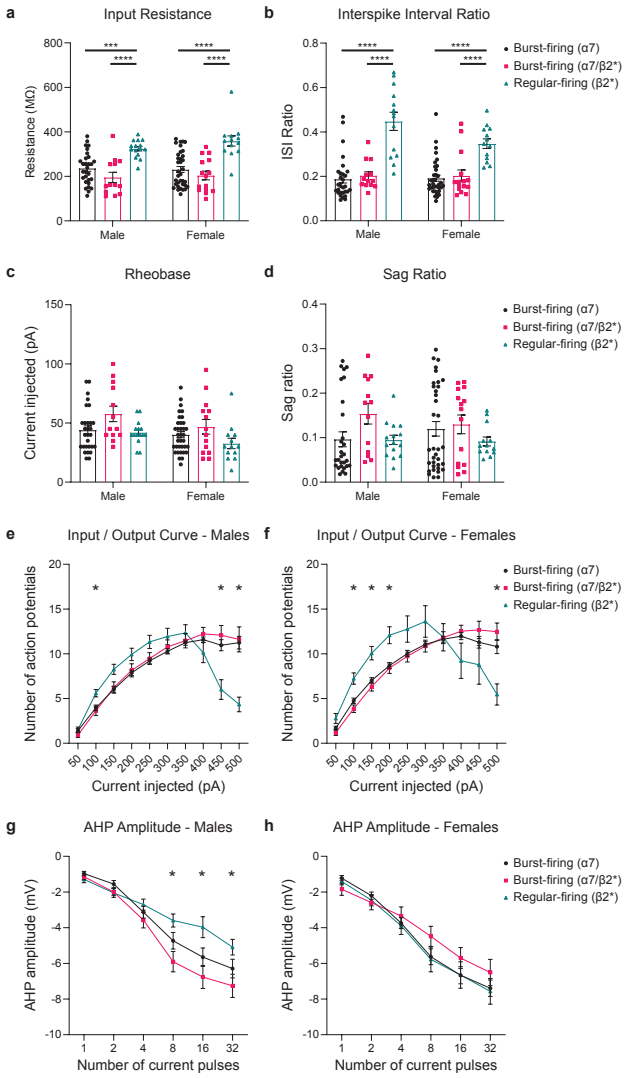

Fig. 3 Characterization of intrinsic electrophysiological properties of prefrontal layer V pyramidal neurons. Input resistance (**a**) showed no sex difference (two-way ANOVA, $p = 0.4$), but was affected by neuron subtype ($p < 0.0001$) with resistance being greatest in regular-firing (β2*) neurons (Bonferroni *post hoc* correction, all $p \leq 0.001$). The same scenario was observed for interspike interval ratio (**b**), which showed no sex difference ($p = 0.09$), but was affected by neuron subtype ($p < 0.0001$) with the interspike interval ratio being greatest in regular-firing (β2*) neurons (all $p \leq 0.001$). Rheobase (**c**) showed a sex difference ($p = 0.02$) and was affected by neuron subtype ($p = 0.008$). Sag ratio (**d**) showed no sex difference ($p = 0.09$) and was not affected by neuron subtype ($p = 0.07$). Input / output curves showed similar effects of neuron subtype within males (**e**) and females (**f**), where two-way ANOVA identified no overall effect of neuron subtype (males: $p = 0.8$; females: $p = 0.2$) but a significant interaction between effects of neuron subtype and the amount of current injected ($p < 0.0001$ for each sex). Firing output was different in regular-firing (β2*) neurons than in the other neuron subtypes where indicated (each $p < 0.05$). A similar scenario was observed for AHP amplitude in males (**g**) and females (**h**), with no overall effect of neuron subtype (males: $p = 0.1$; females $p = 0.7$) but a significant interaction between effects of neuron subtype and the number of current pulses

(males: $p < 0.0001$; females: $p = 0.02$). AHP amplitude was lower in regular-firing ($\beta2^*$) neurons than in burst-firing ($\alpha7/\beta2^*$) neurons for males only (as indicated; each $p < 0.05$). All data are shown for individual neurons and/or as mean +/- 1 SEM. Sample sizes for males are: burst-firing ($\alpha7$) = 29; burst-firing ($\alpha7/\beta2^*$) = 13; regular-firing ($\beta2^*$) = 15, and for females are: burst-firing ($\alpha7$) = 35; burst-firing ($\alpha7/\beta2^*$) = 15; regular-firing ($\beta2^*$) n = 13. Significance levels for Bonferroni *post hoc* corrections within each sex are $^*p < 0.05$, $^{**}p < 0.01$, $^{***}p < 0.001$, and $^{****}p < 0.0001$.

236 **Excitatory presynaptic input to layer V pyramidal neuron subtypes.** The mPFC receives
237 excitatory input from cortical and subcortical sources. We measured the properties of
238 spontaneous excitatory postsynaptic currents (EPSCs) received by the three layer V pyramidal
239 neuron subtypes that were identified in this study. EPSC frequency (Fig. 4a) was affected by
240 neuron subtype (two-way ANOVA, $F(2,113) = 13.41$, $p < 0.0001$), with frequency being lower in
241 RF (β2*) neurons than BF (α7) neurons in both sexes (Bonferroni post hoc correction, $p < 0.01$).
242 Similarly, both EPSC amplitude (Fig. 4b, $F(2,112) = 10.31$, $p < 0.0001$) and net charge (Fig. 4c,
243 $F(2,113) = 17.26$, $p < 0.0001$) were affected by neuron subtype with values being lower in RF
244 (β2*) neurons than in BF (α7) neurons in both sexes (all $p < 0.01$). There was no sex difference
245 for EPSC frequency ($F(1,113) = 0.35$, $p = 0.6$) but there were sex differences for both EPSC
246 amplitude ($F(1,112) = 20.34$, $p < 0.0001$) and net charge $F(1,113) = 19.91$, $p < 0.0001$) in that
247 values were greater in males than females. These results suggest that excitatory synaptic
248 signalling received within mPFC layer V differs depending on pyramidal neuron subtype.

Figure 4

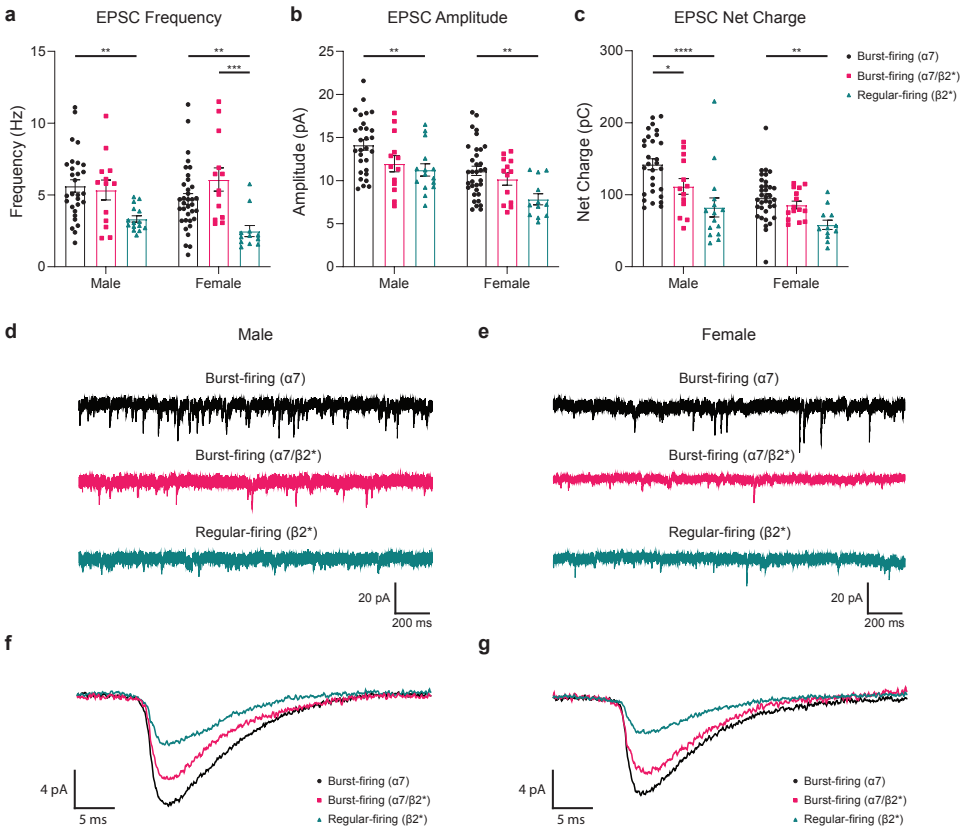

Fig. 4 Characterization of spontaneous presynaptic input to prefrontal layer V pyramidal neurons. Spontaneous EPSC frequency (**a**) showed no sex difference (two-way ANOVA, p = 0.6), but was affected by neuron subtype ($p < 0.0001$) with frequency being lowest in regular-firing (β2*) neurons (Bonferroni *post hoc* correction, $p < 0.01$ or $p < 0.001$ as indicated). EPSC amplitude (**b**) showed a sex difference ($p < 0.0001$) and an effect of neuron subtype ($p < 0.0001$), with amplitude being lowest in regular-firing (β2*) neurons ($p < 0.01$ as indicated). Similarly, EPSC net charge showed a sex difference ($p < 0.0001$) and an effect of neuron subtype ($p < 0.0001$), with net charge being lowest in regular-firing (β2*) neurons ($p < 0.05$, $p < 0.01$, or $p < 0.0001$ as indicated). Typical voltage-clamp traces with EPSCs are shown for one pyramidal neuron from each subtype in males (**d**) and females (**e**). The average of 200 representative EPSCs is shown for pyramidal neurons from each subtype in males (**f**) and females (**g**). All data are shown for individual neurons and as mean +/- 1 SEM. Sample sizes for males are: burst-firing (α7) = 29; burst-firing (α7/β2*) = 13; regular-firing (β2*) = 15, and for females are: burst-firing (α7) = 35; burst-firing (α7/β2*) = 15; regular-firing (β2*) n = 13. Significance levels for Bonferroni *post hoc* corrections within each sex are *$p < 0.05$, **$p < 0.01$, ***$p < 0.001$, and ****$p < 0.0001$.

266 **Correlation between electrophysiological properties and nicotinic responses.** Correlation
267 analyses were performed for all neurons within each sex, to assess relationships between eight
268 intrinsic electrophysiological properties, six measures of nicotinic currents, and three measures
269 of EPSCs. Fig. 5a. shows the resulting correlation matrix for each sex, with positive correlations
270 marked green and negative correlations marked red. Multiple positive correlations were
271 identified that could be expected based on group differences between pyramidal neuron
272 subtypes. For example, input resistance (which was greatest in RF (β2*) neurons) correlated
273 positively with interspike interval adaptation ratio and input/output excitability (which were both
274 greatest in RF (β2*) neurons). Input resistance also correlated positively with measures of
275 nicotinic response kinetics, which were all slower in RF (β2*) neurons. Correlations were
276 identified between measures of nicotinic responses and EPSCs that were not expected. For
277 example, measures of nicotinic response kinetics correlated negatively with EPSC frequency
278 but correlated positively with EPSC amplitude and EPSC net charge.
279 We next assessed potential clustering of recorded neurons into groups using a
280 principal component analysis, for which each of the 17 electrophysiological property, nicotinic
281 response, and EPSC property measures used in the correlation analyses were treated as
282 principal components (PCs). Neurons from male mice had four PCs and neurons from female
283 mice had six PCs with eigenvalues greater than 1, which accounted for 74.2% and 83.2% of the
284 total variance, respectively. A screeplot was used to confirm that a plateau was reached with
285 these PCs and that the remaining PCs did not significantly contribute to group variance. The
286 three PCs with the greatest contribution toward group variance accounted for 37.0%, 15.9%,
287 and 13.1% of total variance in males and 33.4%, 15.1%, and 11.5% of the total variance in
288 females. In both the sexes, the measures that largely contributed to the first PC are nicotinic
289 peak response amplitude (Male: 0.13; Female: 0.14), rise tau (Male: 0.10; Female: 0.12), 1st
290 decay tau (Male: 0.13; Female: 0.14) and 2nd decay tau (Male:0.12; Female: 0.10). Fig. 5b

291 shows three-dimension plots of neurons positioned according to the three largest PCs. Here,
292 neurons separated into two distinct clusters comprising the BF (α7 and α7/β2*) neurons or RF
293 (β2*) neurons. For the BF neuron subtypes, BF (α7) neuron positions were more elongated
294 along the PC2 and PC3 axes, whereas the BF (α7/β2*) neurons formed a tighter cluster within
295 all three axes.

Figure 5

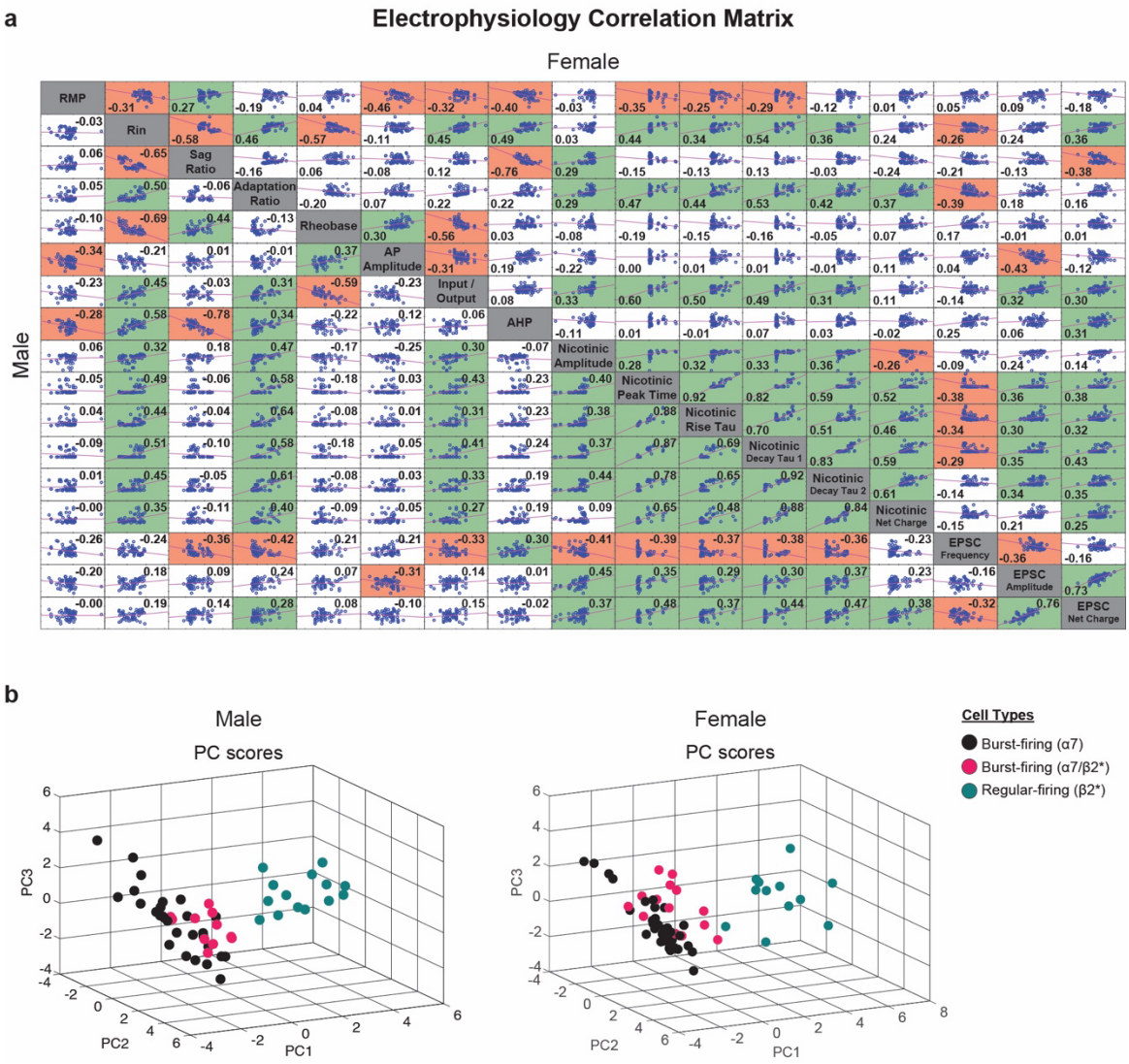

Fig. 5 Correlation and principal component analyses for electrophysiological properties of prefrontal layer V pyramidal neurons. a Correlation matrix comprising eight intrinsic electrophysiological properties, six measures of nicotinic current responses, and three measures of spontaneous EPSCs. Male data is presented on the lower-left and female data is presented on the upper-right. For each comparison, the corresponding cell contains the Pearson correlation coefficient, a graphical representation of the correlation analysis, and the line of best fit. Cells with significant positive correlations are shown in green and cells with significant negative correlations are shown in red (each $p < 0.05$). **b** Principal component analysis included all measures from the correlation matrix. Three-dimension plots are shown for the first three principal components (PCs) that account for 65.9% of variability in males and 60.0% of variability in females. In both sexes, regular-firing (β2*) neurons form an unambiguous cluster separate from the other two burst-firing neuron subtypes. Sample sizes for males are: burst-firing (α7) = 29; burst-firing (α7/β2*) = 13; regular-firing (β2*) = 15, and for females are: burst-firing (α7) = 35; burst-firing (α7/β2*) = 15; regular-firing (β2*) n = 13.

311 **Distinct morphologies of layer V pyramidal neuron subtypes.** The morphology of mPFC
312 layer V pyramidal neuron subtypes has been reported previously[31,32,34,44,45,51]. The morphology
313 of neighbouring mPFC layer VI pyramidal neurons has been related previously with muscarinic[52]
314 and nicotinic[53] responses, so we next sought to determine whether the morphology of mPFC
315 layer V neurons in this study relates with their nicotinic response type. Sholl-type plots were
316 prepared for a random subset of neurons within each sex that were labelled during
317 electrophysiological recording and analysed based on dendrite length (Fig. 6a,b), diameter (Fig.
318 6c,d), and volume (Fig 6e,f).

319 Apical dendrite length showed opposite effects of neuron subtype in each sex. In males,
320 there was a significant effect of neuron subtype (two-way ANOVA, $F(2,520) = 11.99$, $p <$
321 0.0001) with BF (α7) neurons having a smaller length than the other two neuron subtypes
322 (Bonferroni post hoc correction, each $p < 0.01$). In females, there was a significant effect of
323 neuron subtype ($F(2,506) = 16.52$, $p < 0.0001$) with BF (α7) neurons having a greater length
324 than the other two neuron subtypes (each $p < 0.0001$). Basal dendrite length showed similar
325 effects of neuron subtype within males ($F(2,380) = 41.55$, $p < 0.0001$) and females ($F(2,414) =$
326 8.82, $p = 0.0002$). In both sexes, BF (α7) neurons had the greatest basal dendrite length and
327 RF (β2*) neurons had the smallest basal dendrite length. All neuron subtypes were different
328 from each other (each $p < 0.05$) except for the two BF subtypes within females.

329 Apical dendrite diameter showed opposite effects of neuron subtype in each sex. In
330 males, there was a significant effect of neuron subtype ($F(2,520) = 20.81$, $p < 0.0001$) with BF
331 (α7) neurons having a smaller diameter than the other two neuron subtypes (each $p < 0.001$). In
332 females, there was a significant effect of neuron subtype ($F(2,506) = 53.13$, $p < 0.0001$) with BF
333 (α7) neurons having a greater diameter than the other two neuron subtypes (each $p < 0.0001$).
334 Basal dendrite diameter showed an effect of neuron subtype within males ($F(2,380) = 16.65$, $p <$
335 0.0001) with BF (α7) neurons having a greater diameter than the other two neuron subtypes

(each $p < 0.05$). Basal dendrite diameter was not affected by neuron subtype in females ($F(2,414) = 1.60$, $p = 0.2$).

Apical dendrite volume showed opposite effects of neuron subtype in each sex. In males, there was a significant effect of neuron subtype ($F(2,520) = 14.19$, $p < 0.0001$) with BF ($\alpha7$) neurons having a smaller volume than BF ($\alpha7/\beta2^*$) neurons ($p < 0.0001$). In females, there was a significant effect of neuron subtype ($F(2,506) = 65.19$, $p < 0.0001$) with BF ($\alpha7$) neurons having a greater volume than the other two neuron subtypes (each $p < 0.0001$). Basal dendrite volume showed similar effects of neuron subtype within males ($F(2,380) = 18.79$, $p < 0.0001$) and females ($F(2,414) = 25.46$, $p < 0.0001$), with RF ($\beta2^*$) neurons having a smaller basal dendrite volume than the other two neuron subtypes (each $p < 0.001$).

Figure 6

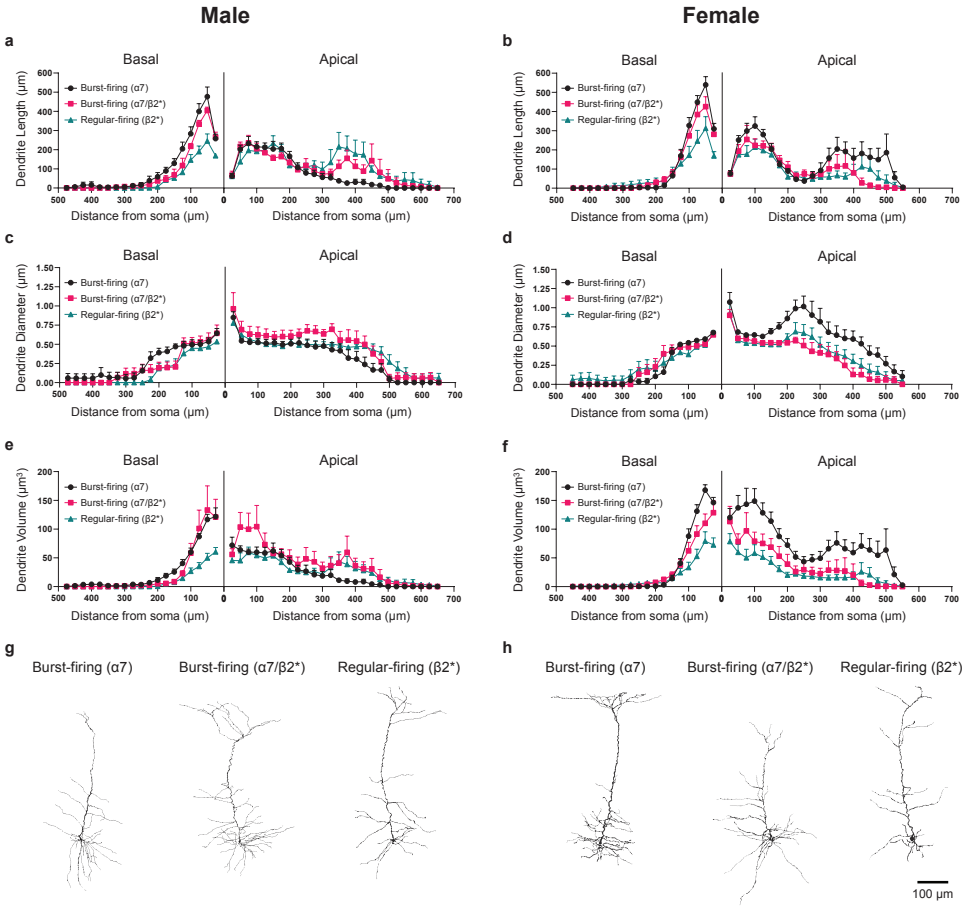

Fig. 6 Dendrite morphology of prefrontal layer V pyramidal neurons. Sholl plots are shown for dendrite length, diameter, and volume as a function of distance from neuron soma. Data are shown for males on the left side of the figure and for females on the right side of the figure. For each plot, apical dendrite data is oriented to the right of zero, and basal dendrite data is oriented to the left of zero, with zero indicating the location of the soma. Apical dendrite length showed an effect of neuron subtype for both males (**a**) and females (**b**) (two-way ANOVA, each $p < 0.0001$). Burst-firing (α7) neurons showed the lowest apical length in males (Bonferroni *post hoc* correction, $p \leq 0.05$) and the greatest apical length in females ($p < 0.0001$). Basal dendrite length showed an effect of neuron subtype in both sexes ($p \leq 0.001$) with the lowest basal length in regular-firing (β2*) neurons ($p \leq 0.05$). Apical dendrite diameter showed an effect of neuron subtype in males (**c**) and females (**d**) (each $p < 0.0001$) whereas basal dendrite diameter showed an effect of neuron subtype in males only ($p < 0.0001$). Apical dendrite volume showed an effect of neuron subtype for both males (**e**) and females (**f**) (each $p < 0.0001$). Burst-firing (α7/β2*) neurons showed the greatest apical dendrite volume in males ($p \leq 0.001$) whereas burst-firing (α7) neurons showed the greatest apical dendrite volume in females ($p < 0.0001$). Basal dendrite volume showed an effect of neuron subtype in both sexes ($p \leq 0.0001$) with the lowest basal dendrite volume in regular-firing (β2*) neurons ($p \leq 0.001$). Sample sizes for males are: burst-firing (α7) = 9; burst-firing (α7/β2*) = 6; regular-firing (β2*) = 7, and for females are: burst-firing (α7) = 11; burst-firing (α7/β2*) = 6; regular-firing (β2*) n = 8. Typical traces of reconstructed pyramidal neurons are shown for males (**g**) and females (**h**) below the Sholl plots for each sex. The scale bar represents 100 μm.

368 **Sex differences in the morphology of layer V pyramidal neuron subtypes.** We performed a
369 direct comparison of dendrite volume between male and female pyramidal neurons sampled
370 from each subtype. The most striking sex difference was observed for BF (α7) neurons, where
371 apical (two-way ANOVA, $F(1,468) = 110.20$, $p < 0.0001$) and basal ($F(1,342) = 5.57$, $p = 0.02$)
372 dendrites had a greater volume in females (Fig. 7a). On the contrary, there was no sex
373 difference for BF (α7/β2*) neuron apical ($F(1,213) = 3.69$, $p = 0.06$) or basal ($F(1,228) = 0.03$, p
374 $= 0.9$) dendrites (Fig. 7b). There were subtle sex differences in RF (β2*) neurons, where apical
375 dendrites had a greater volume in males ($F(1,338) = 4.77$, $p = 0.03$) and basal dendrites had a
376 greater volume in females ($F(1,247) = 11.82$, $p = 0.0007$) (Fig. 7c). These results demonstrate
377 that the morphology of certain mPFC layer V pyramidal neuron subtypes differs between the
378 sexes during the juvenile period.

Figure 7

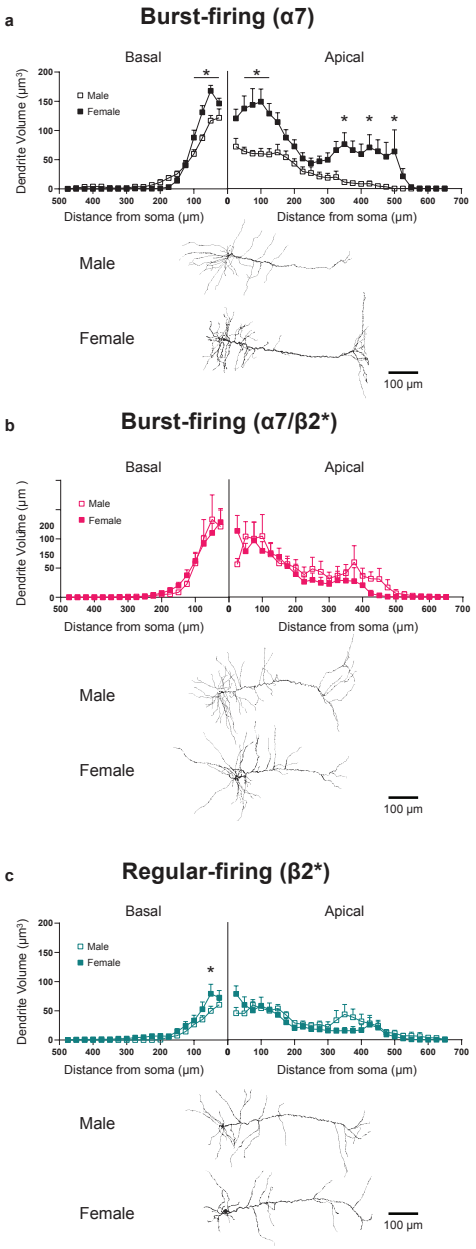

Fig. 7 Sex differences in the morphology of prefrontal layer V pyramidal neurons. Sholl plots are shown comparing male and female dendrite volume for each of the pyramidal neuron subtypes. For each plot, apical dendrite data is oriented to the right of zero, and basal dendrite data is oriented to the left of zero, with zero indicating the location of the soma. **a** In burst-firing (α7) neurons, apical dendrite volume showed a sex difference (two-way ANOVA, p <0.0001) that depended on the distance from the soma (interaction effect, p = 0.005). Apical dendrites from females had a greater volume than those from males (Bonferroni *post hoc* correction, p < 0.05 as indicated). Basal dendrite volume also showed a sex difference (p = 0.02) that depended on the distance from the soma (p < 0.0001). **b** In burst-firing (α7/β2*) neurons, there was no sex difference for apical dendrite volume (p = 0.06) or for basal dendrite volume (p =

0.9). **c** In regular-firing (β2*) neurons, both apical dendrite volume (p = 0.03) and basal dendrite volume (p = 0.0007) showed a significant sex difference with no dependence on distance from the soma (both p = 0.6). Basal dendrite volume was greater in females, as indicated. Sample sizes for males are: burst-firing (α7) = 9; burst-firing (α7/β2*) = 6; regular-firing (β2*) = 7, and for females are: burst-firing (α7) = 11; burst-firing (α7/β2*) = 6; regular-firing (β2*) n = 8. All data are shown as mean +/- 1 SEM. *p < 0.05 for a significant sex difference following Bonferroni *post hoc* corrections. Typical traces of reconstructed neurons from each sex are shown below each Sholl plot. The scale bars represent 100 μm.

398 **Brain region projection targets of layer V pyramidal neuron subtypes.** Previous work has
399 demonstrated that electrophysiological and/or morphological properties of mPFC layer V
400 pyramidal neurons are related with their axonal projection targets[32,44,45]. We next used a
401 retrograde labelling approach to determine whether the mPFC layer V pyramidal neuron
402 subtypes identified in this current study, based on action potential firing patterns and nicotinic
403 response types, also exhibit distinct axonal projection targets. A retrograde tracer was injected
404 into the contralateral mPFC, ipsilateral ventral striatum (nucleus accumbens), or ipsilateral
405 ventromedial thalamus in mice of both sexes at P18 and labelled mPFC layer V pyramidal
406 neurons were recorded for whole cell electrophysiology at P21. Neurons were recorded from 3-
407 4 mice per projection target per sex. The results from this experiment confirm that each neuron
408 subtype projects to a distinct cortical or sub-cortical target. All recorded cortico-cortical neurons
409 projecting to the contralateral mPFC had electrophysiological properties consistent with the BF
410 (α7) subtype (Fig. 8a), as they exhibited a BF action potential firing pattern and a nicotinic
411 response with a fast onset and one-component fast decay. These properties were observed in
412 10/10 neurons from males and 10/10 neurons from females. All recorded cortico-striatal
413 neurons projecting to the ipsilateral nucleus accumbens had electrophysiological properties
414 consistent with the BF (α7/β2*) subtype (Fig. 8b), as they exhibited a BF action potential firing
415 pattern and a nicotinic response with a fast onset and two-component fast plus slow decay.
416 These properties were observed in 10/10 neurons from males and 10/10 neurons from females.
417 In a separate set of animals, retrograde labelling showed that neurons projecting to the
418 caudate/putamen, basolateral amygdala, and lateral hypothalamus also all had
419 electrophysiological properties consistent with the BF (α7/β2*) subtype, suggesting that neurons
420 from this subtype may project to multiple targets. All recorded cortico-thalamic neurons
421 projecting to the ipsilateral ventromedial thalamus had electrophysiological properties consistent
422 with the RF (β2*) subtype (Fig. 8c), as they exhibited a RF response to positive current injection

423 and a nicotinic response with a slow onset and one-component slow decay. These properties

424 were observed in 12/12 neurons from males and 12/12 neurons from females.

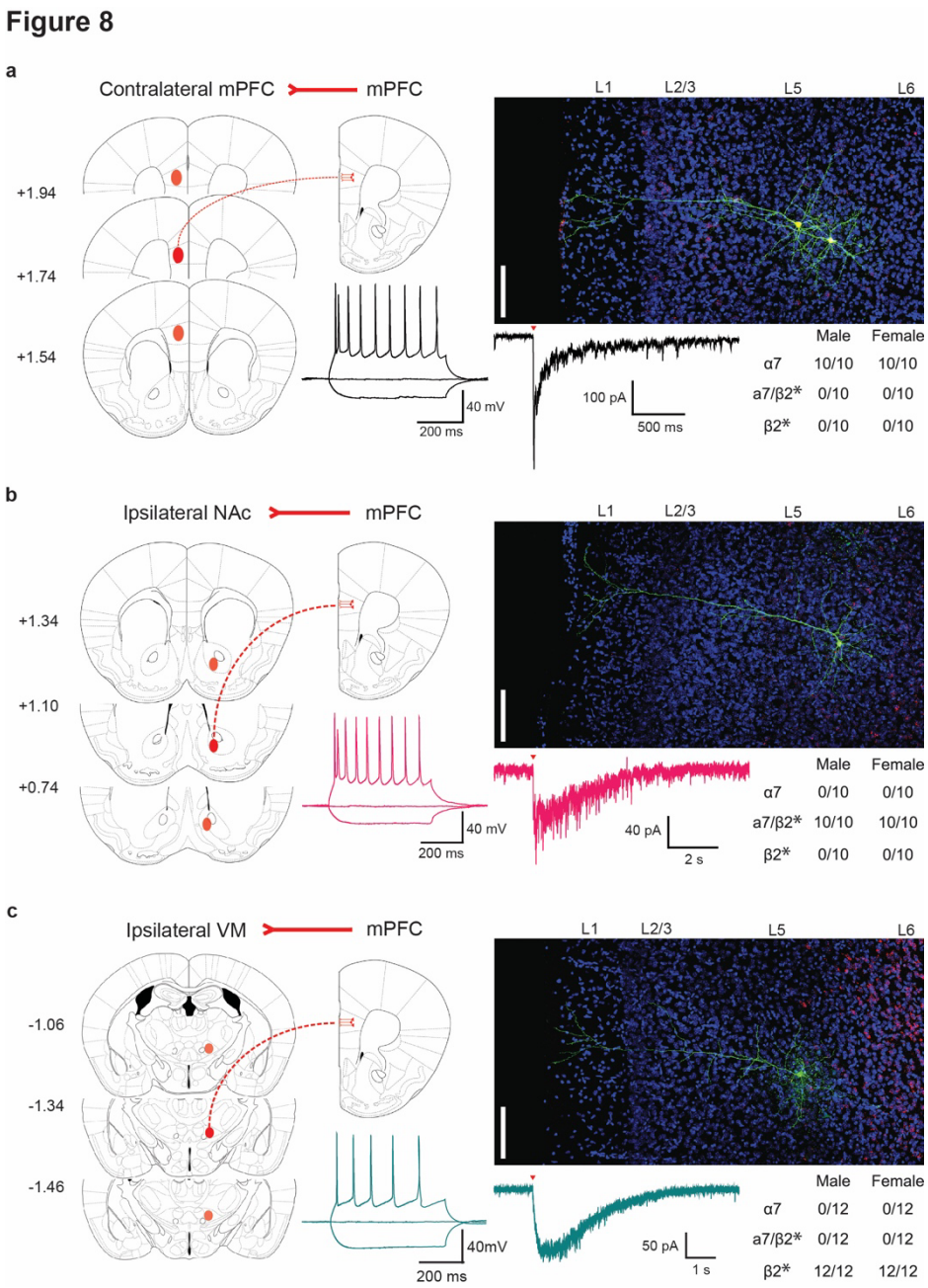

Fig. 8 Retrograde labelling of prefrontal layer V pyramidal neurons. Prefrontal layer V pyramidal neurons were recorded after intracranial injection of retrograde tracer into the (**a**) contralateral mPFC, (**b**) ipsilateral nucleus accumbens, or (**c**) ipsilateral ventromedial thalamus. For each injection region, coronal diagrams relative to bregma show the injection site in red. Representative photomicrographs of the mPFC show DAPI-stained nuclei (blue), retrograde tracer (red), and layer V pyramidal neurons containing the retrograde tracer that were recorded for electrophysiology and filled with biocytin (green). For the contralateral mPFC, all retrograde-labelled neurons that were recorded showed a burst-firing response to 200 pA of positive current and an α7 nicotinic response to 1 mM ACh (indicated by the red arrowhead). No other nicotinic response was observed. For the ipsilateral nucleus accumbens, all retrograde-labelled neurons that were recorded showed a burst-firing response to 200 pA of positive current and an

437 α7/β2* nicotinic response to 1 mM ACh. For the ipsilateral ventromedial thalamus, all
438 retrograde-labelled neurons that were recorded showed a regular-firing response to 200 pA of
439 positive current and a β2* nicotinic response to 1 mM ACh. The contingency table presented for
440 each injection region shows the proportion of recorded neurons that showed each nicotinic
441 response type. Scale bars on the photomicrographs represent 100 μm.

442 **Discussion**

443 Layer V pyramidal neurons play a central role within mPFC cognitive circuits. They span the
444 cortical column, integrate afferent signals from cortical and subcortical sources[54], and send
445 efferent signals to cortical and subcortical targets[55]. Their role to support cognitive functions is
446 modulated by cholinergic neurotransmission that involves postsynaptic nicotinic
447 responses[16,18,56]. Characterizing the manner by which nicotinic signalling modulates mPFC layer
448 V neurons in juvenile age mice is important for understanding the role of cholinergic
449 neurotransmission in the maturation and function of mPFC-associated circuits. In this present
450 study, we report the following for mPFC layer V pyramidal neurons sampled from juvenile age
451 mice: 1) Unique nAChR isoform-specific nicotinic responses are present in distinct subtypes of
452 neurons; 2) these neuron subtypes exhibit distinct combinations of intrinsic electrophysiological
453 and morphological properties, and axonal projection targets, which are largely consistent with
454 previous reports; 3) these neuron subtypes exhibit distinct levels of spontaneous presynaptic
455 excitatory input; and 4) strong correlations exist between measures of nicotinic responses and
456 certain intrinsic electrophysiological properties. A graphical summary of neuron populations
457 expressing α7 and β2* nAChRs within all layers of the mPFC is presented in Fig. 9, based on
458 findings from this current study and previous reports.

459

Figure 9

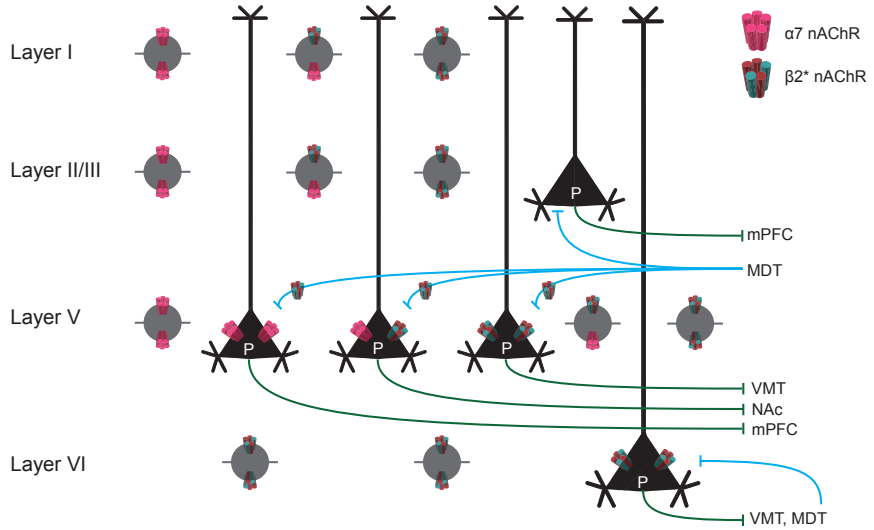

460

461 **Fig. 9 Graphical summary of nicotinic receptor localization within the prefrontal cortex.**
462 Based on previous literature and the findings from this current study, α7 and β2 subunit-
463 containing nAChRs are expressed at distinct sites within the juvenile rodent medial prefrontal
464 cortex. The majority of pyramidal neurons (P) in layers II/III do not appear to express nAChRs.
465 Pyramidal neurons in layer V may be categorized into three subtypes based on this current
466 study that express α7 and/or β2* nAChRs. Pyramidal neurons in layer VI express β2* nAChRs
467 only. Interneurons in layers I, II/III, and V express α7 and/or β2* nAChRs, whereas interneurons
468 in layer VI express β2* nAChRs only. Glutamatergic inputs from the mediodorsal thalamus to
469 layer V pyramidal neurons also express β2* nAChRs. Glutamatergic inputs to the mPFC are
470 shown in blue and outputs to specified projection targets are shown in green. Not all input or
471 output pathways from the mPFC are shown. mPFC, medial prefrontal cortex; MDT, mediodorsal
472 thalamus; VMT, ventrolateral thalamus; NAc, nucleus accumbens.

473 The functional presence of nAChR isoforms has been characterized previously for specific
474 neuron types within each layer of the rodent mPFC[16,17,57,58]. That work shows α7 nAChRs to be
475 present on fast spiking and non-fast spiking interneurons within layers I, II/III, and V, on a
476 minority of pyramidal neurons within layer II/III, and on the majority of pyramidal neurons within
477 layer V [16,57,58]. It also shows β2* nAChRs to be present on thalamocortical glutamatergic
478 terminals within layer V[59], fast spiking interneurons within layer V[17], non-fast spiking
479 interneurons within all layers[16,58], and on pyramidal neurons within layer VI only[16,53,60]. Our
480 finding that nicotinic responses mediated by β2 subunit-containing nAChRs are present in
481 approximately half of recorded BF neurons (α7/β2* nicotinic responses) and all of recorded RF
482 neurons (β2* nicotinic responses) is not consistent with previous reports described above for
483 mPFC layer V. A possible explanation for this inconsistency could be that we had actually
484 recorded α7, α7/β2*, and β2* nicotinic responses in non-fast spiking interneurons as reported
485 previously for this layer[16]. However, we are confident that we recorded from pyramidal neurons
486 only, based on their characteristic action potential firing patterns, prominent apical dendrite
487 morphology, and retrograde-labelled projections to known callosal and subcortical targets.
488 Differences in study design or recording conditions could underlie differences between our
489 findings and previous reports. The work described above was performed using mice and rats of
490 approximately the same developmental age as those in our study but was performed at a
491 greater recording temperature than our study. Although recording temperature can transform
492 action potential firing patterns between BF and RF for pyramidal neurons[61], we have found that
493 temperature does not influence apparent nAChR isoform-specific response types within the
494 pyramidal neurons of our study. Another potential difference between our study and previous
495 research is the mPFC sub-region from which neurons were sampled (i.e., the prelimbic or
496 infralimbic regions). Neurons in our study were sampled from the prelimbic region only, whereas
497 most previous reports do not state the sub-region from which neurons were sampled. There

498 may be sex differences in nAChR expression or function in mPFC layer V, although we did not
499 observe this for most measures of nAChR function in our study. Previous studies were
500 performed in males only, combined males and females, or did not report the sex of experimental
501 animals. Consistent with our findings, it should be noted that β2* nicotinic responses have been
502 observed in layer V pyramidal neurons located within the rat somatosensory[18] and mouse
503 auditory[62] cortices. However, details of these studies suggest that the mapping of isoform-
504 specific nicotinic response types to specific pyramidal neuron subtypes may differ between the
505 mPFC and primary sensorimotor cortices. For example, both α7 and β2* responses were
506 observed in RF neurons of the somatosensory cortex[18], and β2* responses were observed in
507 both cortico-cortical and cortico-collicular neurons of the auditory cortex[62].
508 Beyond the broad observation that nicotinic responses mediated by multiple nAChR
509 isoforms are present in mPFC layer V pyramidal neurons, we show further that each unique
510 nicotinic response type is present in a distinct neuron subtype. The neuron subtypes that we
511 identified exhibit properties that are largely consistent with those described in previous reports
512 for the mPFC. Based on axonal projection targets, IT neurons projecting within the contralateral
513 cortex or to the striatum tend to show a BF action potential firing pattern and have a thinner
514 apical dendrite tuft, compared with PT neurons projecting to subcortical regions that tend to
515 show an RF action potential firing pattern and have a wider apical dendrite tuft[32,38,44,45,63]. Also
516 consistent with our findings, Wang and colleagues[34] found non-accommodating RF neurons
517 with complex/wide apical dendrite tufts and accommodating BF neurons with simple/narrow
518 apical dendrite tufts. This previous work largely matches the properties of neuron subtypes
519 identified for male mice in our study, and only differs from female mice in our study with regard
520 to their wide apical dendrite tuft for BF (α7) neurons. van Aerde and Feldmeyer[31] identified
521 neuron subtypes in rat mPFC based on action potential firing pattern and apical dendrite
522 morphology, but observed the BF doublet only in a small fraction of neurons, and instead sub-

523 divided RF neurons into adapting/non-adapting groups. Multiple aspects of experimental design
524 differed between that study and ours, including species (rat), sex (both combined), age (P24-46)
525 and recording temperature (30°C). The physiology and morphology of pyramidal neurons are
526 well known to change during postnatal maturation into adulthood. Although the proportion of IB
527 and RF layer V pyramidal neurons shifts between P18-22 and adulthood for the rat
528 sensorimotor cortex[23], the action potential firing patterns and apical dendrite morphology do not
529 appear to differ between P13-16 and P26-30 in the mouse mPFC[51]. Shifting from room
530 temperature to physiological temperature can shift the action potential firing pattern for layer V
531 pyramidal neurons from IB to RF[61], so it is possible that our recordings at room temperature do
532 not reflect the neurons' true action potential firing patterns *in vivo*. Notwithstanding this, our
533 experimental design allowed us to identify the distinct neuron subtypes that were then
534 characterized through their distinct nicotinic response types, morphology, and projection targets.
535 Properties of the layer V pyramidal neuron subtypes themselves seem to differ between the
536 mPFC and primary sensorimotor cortices, where BF neurons typically have thick apical dendrite
537 tufts and project to PT targets whereas RF neurons typically have thin apical dendrite tufts and
538 project to IT targets (see Introduction).

539 The most striking sex difference observed in this study was the greater apical and basal
540 dendrite length and volume measured in BF (α7) neurons from female mice (Fig. 7a), which is
541 not consistent with the greater EPSC amplitude and net charge measured in BF (α7) neurons
542 from male mice (Fig. 4b, c). Other measures of intrinsic electrophysiological properties that may
543 reflect neuron size (e.g. input resistance and rheobase) did not differ between sexes for this
544 neuron type. These data suggest that neurons from male mice may be coupled with presynaptic
545 glutamatergic input more efficiently in males than in females, or that the quantal release of
546 glutamate is greater in males than in females, at this age. The only sex difference that we
547 observed for nicotinic responses was the greater net charge of β2* nicotinic responses in

548 neurons from male mice, which resulted from the slower response decay kinetics in this sex. We
549 observed no sex difference in α7 or α7/β2* nicotinic responses. In neighbouring layer VI
550 pyramidal neurons from the juvenile mouse mPFC, the β2* nicotinic response amplitude was
551 reported to be greater in males than in females[60].

552 We observed that nicotinic response types are related with apical dendrite morphology in
553 a sex-dependent manner for mPFC layer V pyramidal neurons during the juvenile period of
554 postnatal development. Nicotinic α7 responses map onto narrow tufted neurons in males and
555 wide tufted neurons in females, whereas α7/β2* and β2* responses map onto neurons that are
556 relatively wide tufted in males and narrow tufted in females. Cholinergic[64], nicotinic[53], and
557 muscarinic[52] signalling has been related with apical dendrite morphology for pyramidal neurons
558 within other layers of the mPFC. It cannot be determined based on our data whether the nAChR
559 isoform-specific nicotinic responses play a role to shape the dendrite morphology of the layer V
560 pyramidal neuron subtypes identified in this study, although this would be an interesting avenue
561 for future research.

562 Pyramidal neurons within layer V of the mPFC provide the primary output signal from
563 this region and project to a wide variety of targets within limbic-cognitive circuits, including the
564 mPFC itself and other regions of the cerebral cortex, ventral striatum (nucleus accumbens),
565 dorsal striatum (caudate/putamen), thalamus, lateral hypothalamus, basolateral amygdala,
566 ventral tegmental area, and brainstem/spinal cord[55,65,66]. Pyramidal neuron subtypes likely have
567 specific roles to support cognitive functions, depending on their projection targets, intrinsic
568 electrophysiological properties, and postsynaptic neurotransmitter receptors. In dorsal cortical
569 regions, subtypes of IT and PT neurons show unique activity during, and contributions toward,
570 an auditory decision task, with PT neurons making the greatest contribution[67,68]. In the mPFC,
571 layer V pyramidal neurons projecting to the dorsal striatum contribute toward cognitive
572 flexibility[69] and inhibitory control[70], while those projecting to the mediodorsal thalamus contribute

573 toward attention and inhibitory control depending on the specific target within that brain region[70].
574 Regarding action potential firing patterns, it is the output from prefrontal BF neurons that is
575 thought to synchronize this region during attention tasks[71,72]. Attention performance likely is
576 supported by phasic[5] and tonic[4] ACh neurotransmission. Since nAChR activation and
577 desensitization kinetics differ between nAChR isoforms, with faster activation and
578 desensitization in α7 nAChRs than β2* nAChRs (reviewed in Papke and Lindstrom[73]), the
579 presence of unique isoform-specific nicotinic responses in distinct pyramidal neuron subtypes
580 likely influences their cellular response to ACh thereby shaping their distinct contributions
581 toward mPFC-dependent and ACh-supported cognitive tasks.

582 **Methods**

583 **Experimental animals**

584 All experiments were performed using CD1-strain mice in accordance with the principles and
585 guidelines of the Canadian Council on Animal Care, and under protocols that were approved by
586 the University of Guelph Animal Care Committee. Pregnant mice were purchased from Charles
587 River Canada (Saint-Constant, Quebec, Canada) and used to establish a local breeding colony.
588 Mice were housed at an ambient temperature of 21-24°C with lights maintained on a 12-hour
589 cycle (lights on at 8:00 pm) and were provided *ad libitum* access to food and water.

590

591 **Whole-cell electrophysiology in acute brain slices**

592 Male and female mice between postnatal day (P) 15-20 were anesthetized using isoflurane and
593 killed by decapitation. Whole brains were rapidly removed under 4°C oxygenated sucrose
594 artificial cerebrospinal fluid (sACSF) (in mM: 245 sucrose, 10 D-Glucose, 26 $NaHCO_3$, 2 $CaCl_2$,
595 2 $MgSO_4$, 3 KCl, and 1.25 NaH_2PO_4, pH 7.4). Coronal slices containing the mPFC from
596 approximately Bregma +1.98 mm to +1.34 mm[74] were made at 400 μm thickness using a Leica
597 VT1200 vibrating microtome (Leica Microsystems Inc., Concord, Ontario, Canada). Slices were
598 transferred to a recovery chamber containing oxygenated regular ACSF (in mM; 128 NaCl, 10 D-
599 glucose, 26 NaH_2CO_3, 2 $CaCl_2$, 2 $MgSO_4$, 3 KCl, and 1.25 NaH_2PO_4, pH 7.4) and maintained at
600 30°C for at least two hours prior to electrophysiology recordings.

601 Slices were transferred to a recording chamber (Warner Instruments, Hamden,
602 Connecticut, USA), superfused with fresh oxygenated ACSF at room temperature, and
603 visualized by infrared differential interference contrast microscopy using an Axioskop FS2
604 microscope (Carl Zeiss Canada, Toronto, Ontario, Canada). Layer V pyramidal neurons were
605 sampled for recording randomly within layer V of the prelimbic region, based on their location
606 approximately 300-550 μm from the pial surface[16], large soma size, pyramidal shape, and
607 prominent apical dendrite projecting toward the pial surface. Whole-cell electrophysiological

608 recordings were conducted using borosilicate glass electrodes having an internal resistance of
609 3-5 MΩ (Sutter Instrument Company, Novato, California, USA, catalogue number BF150-110-
610 10). The electrode solution contained (in mM): 120 K-gluconate, 5 KCl, 2 $MgCl_2$, 4 K_2-ATP, 0.4
611 Na_2-GTP, 10 Na_2-phosphocreatine, 10 HEPES buffer (pH 7.3). Recordings were made using a
612 Multiclamp 700B amplifier (Molecular Devices, San Jose, California, USA), with signals acquired
613 at 20 kHz and low-pass filtered at 2 kHz using a Digidata 1440A digitizer (Molecular Devices).
614 The liquid junction potential was corrected at the time of recording.
615
616 **Measurement of intrinsic electrophysiological properties**
617 Neuron intrinsic electrophysiological properties were first measured in current clamp mode.
618 Resting membrane potential was measured shortly after the whole-cell configuration was
619 achieved with no current injection. Input resistance was calculated based on the change in
620 membrane potential from rest in response to 500 ms of -100 pA current. Inter-spike interval (ISI)
621 ratio was used to assess spike frequency adaptation and was calculated as the ratio of
622 durations between the first two action potentials and last two action potentials generated in
623 response to 500 ms of +200 pA current. Sag ratio was calculated as the ratio between the
624 lowest membrane potential and the steady-state membrane potential generated in response to
625 500 ms of -100 pA current. Rheobase was measured by injecting 500 ms of positive current that
626 increased in magnitude by 5 pA with each step until a single action potential was elicited. Action
627 potential amplitude was measured at rheobase as the difference between the threshold
628 potential and the peak potential. Postburst afterhyperpolarization (AHP) responses were
629 measured as the difference between the resting membrane potential and the lowest membrane
630 potential attained after injection of 1, 2, 4, 8, 16, and 32 current pulses (2 ms, 2 nA, at 50 Hz).
631 Input/output curves were generated by measuring the number of action potentials elicited in
632 response to 500 ms positive current steps that increased in 50 pA increments.
633

634 **Measurement of spontaneous excitatory postsynaptic currents**

635 Spontaneous EPSCs were recorded in voltage-clamp mode at a holding potential of −75 mV for
636 a 30s period. Tracings were analyzed offline using a template search in Clampfit software
637 (version 10, Molecular Devices). Events that were <5 or >100 pA were not included in the
638 analysis. EPSC frequency, amplitude, and net charge were measured.

639

640 **Measurement of postsynaptic nicotinic currents**

641 Postsynaptic nicotinic currents were measured in voltage-clamp mode at -75 mV in the
642 presence of 200 nM atropine to inhibit muscarinic receptors. 1 mM ACh was prepared in ACSF
643 within a borosilicate glass application pipette having a resistance of 3-5 MΩ and pressure
644 applied at 10 psi for 100 ms using a Picospritzer II (General Valve, Fairfield, New Jersey, USA).
645 Relative to the soma, the application pipette was positioned 20-50 μm upstream and at a 45
646 degree angle from the flow of ACSF within the recording chamber. Initial experiments in Fig. 1
647 were performed in the presence of 10 nM MLA citrate (Tocris / Bio-Techne Canada, Toronto,
648 Ontario, Canada) and/or 3 μM DHβE hydrobromide (Tocris) to determine the contribution of α7
649 and β2 subunit-containing nAChRs, respectively. Pressure application of ACSF alone did not
650 alter the holding currents in these experiments.

651 Nicotinic currents were measured using a custom-written program in MATLAB (version
652 9.7, MathWorks, Natick, Maine, USA). Current amplitude, net charge, response time, rise and
653 decay kinetics were used to characterized nicotinic currents mediated by α7, α7/β2*, and β2*
654 responses (Fig. 2). Rise and decay kinetics were analyzed separately using nonlinear least-
655 squares curve fitting via an eight-term Fourier series equation. Nicotinic currents mediated by α7
656 and β2* responses were distinguishable based on rise and decay kinetics, which were
657 significantly more rapid for α7 responses than for β2* responses. In the subset of neurons that
658 exhibited nicotinic currents mediated by α7/β2* responses, the second decay tau ($D\tau_2$) threshold
659 of 930 ms was used to distinguish between currents mediated by α7 and α7/β2* responses.

660

661 **Correlation matrix and principal component analysis**

662 A total of eight measures of intrinsic electrophysiological properties, six measures of nicotinic
663 currents, and three measures of EPSCs were used to generate a correlation matrix and perform
664 principal component analysis within each sex (Fig. 5). The Pearson correlation coefficient and
665 its associated *p* value were calculated for each possible pair of measures for all neurons
666 irrespective of their nicotinic current response type. Principal component analysis was used to
667 visualize the distribution of neuron subtypes (categorized based on nicotinic responses) in
668 multidimensional space. The Kaiser-Gutman criterion was used to decide the initial number of
669 PCs. Only PCs with an eigenvalue equal to or greater than one were selected for subsequent
670 analysis. The selection of significant PCs was confirmed using a scree plot of all PCs.
671 Significant PCs were then used to produce a three-dimension scatterplot matrix.

672

673 **Visualization and measurement of neuron morphology**

674 During electrophysiological recordings, a subset of neurons exhibiting each type of nicotinic
675 response were labelled with 0.3% (wt/vol) biocytin (Tocris) in the electrode solution. Brain slices
676 were fixed in 4% (wt/vol) paraformaldehyde in 100 mM phosphate buffer (pH 7.5) for up to 3
677 weeks at 4°C. Slices were washed in Tris-buffered saline (TBS, 100 mM Tris and 150 mM NaCl,
678 pH 7.5) 3 x 10 min at room temperature and incubated with 0.5% (vol/vol) H_2O_2 and 0.25%
679 (vol/vol) Triton X-100 in TBS for 15 min at room temperature. Slices were washed in TBS 3 x 10
680 min at room temperature and incubated with 0.25% (vol/vol) VECTASTAIN Elite reagent A
681 (avidin), 0.25% (vol/vol) VECTASTAIN Elite reagent B (biotinylated horseradish peroxidase),
682 and 0.25% (vol/vol) Triton X-100 in TBS for 24 hours at room temperature (Vector Labs,
683 Burlingame, California, USA). Slices were washed in TBS 3 x 10 min at room temperature and
684 incubated with 0.05% (wt/vol) 3,3′-diaminobenzidine tetrahydrochloride hydrate (DAB), 0.04%
685 (wt/vol) nickel chloride hexahydrate, and 0.25% (vol/vol) Triton X-100 in TBS for 5 min at room

686 temperature. Slices were then incubated in this same DAB/nickel/Triton X-100 solution that also
687 contained 0.001% (vol/vol) H_2O_2 for 15 minutes at room temperature. The reaction was stopped
688 by washing slices 3 x 10 min in TBS at room temperature, after which slices were mounted onto
689 microscope slides and allowed to air dry. Slides were dehydrated through ethanol gradients and
690 coverslipped using Permount (Fisher Scientific, Ottawa, Ontario, Canada).

691 Individuals involved in neuron imaging and analysis were blinded to the experimental
692 groups. Brightfield image stacks containing labelled neurons were captured using an Olympus
693 BX53 upright microscope equipped with an Olympus UPlanSApo 30x / 1.05 N.A. silicone-
694 immersion objective (Olympus Canada Inc., Richmond Hill, Ontario, Canada), which was
695 controlled by Neurolucida software (MBF Bioscience, Williston, Vermont, USA). Labelled
696 pyramidal neurons were reconstructed and measured only if they contained one prominent
697 apical dendrite that projected toward the pial surface and all dendrites were fully contained
698 within the slice. Neurons were reconstructed in three dimensions using Neuromantic software[75]
699 and their morphology was measured using Neurolucida Explorer software (MBF Bioscience).
700 Modified Sholl analyses were conducted separately on apical and basal dendrites, in which the
701 length, diameter, and volume of dendrites were measured between concentric spheres radiating
702 from the soma in 25 μm increments.

703

704 **Retrograde labelling**

705 Male and female mice underwent retrograde labelling surgery on P18. Three-to-four mice were
706 used for each sex and labelling region. Carprofen was administered s.c. to the back at 20 mg/kg
707 one hour before surgery. Mice were anaesthetised using isoflourane and placed in a stereotaxic
708 apparatus (David Kopf Instruments, Tujunga, California, USA). The scalp was shaved and
709 anesthetized with the s.c. administration of 50 μL of a local anesthetic cocktail containing 0.67%
710 lidocaine and 0.17% bupivacaine, made from stock solutions in a volumetric ratio of 3:6:9
711 lidocaine:bupivacaine:saline. The scalp was cut along the midline and a small hole was drilled in

712 the skull above the labelling region of interest. Relative to bregma, coordinates for each labelling
713 region were: mPFC: AP: 1.8 mm, ML: -0.35 or 0.35 mm, DV: -2.6 mm, nucleus accumbens: AP:
714 1.1 mm, ML: -2.6 or 2.6 mm, DV -3.9 mm; 15° angle from vertical, and ventromedial thalamus:
715 AP: -1.3 mm, ML: -0.75 or 0.75 mm, DV: -4.2 mm. A custom microinjector delivered 0.3 µL of
716 rhodamine-labelled RetroBeads (0.5x dilution; LumaFluor Inc., Durham, North Carolina, USA)
717 into the labelling region at a rate of 0.1 µL/min using infusion pump (model PHD 2000; Harvard
718 Apparatus, Holliston, Maine, USA). Microinjectors were left in place for an additional 10 minutes,
719 after which they were removed slowly and exposed skull was covered with dental cement. Mice
720 were returned to their home cage for at least 48 h and killed for electrophysiology experiments
721 at P20-21 as described above. Coronal brain sections containing the mPFC were visualized
722 using widefield fluorescence and retrograde-labelled pyramidal neurons were assessed for
723 physiology and morphology using whole-cell electrophysiology with biocytin labelling.
724
725 **Confocal Microscopy**
726 After recording of retrograde-labelled neurons, brain slices were fixed in 4% (wt/vol)
727 paraformaldehyde in 100 mM phosphate buffer overnight at 4°C. Slices were washed in TBS 3 x
728 10 min at room temperature and incubated in blocking buffer comprising 10% (wt/vol) bovine
729 serum albumin (BSA) and 0.25% (vol/vol) Triton X-100 in TBS for two hours at room
730 temperature. Slices were washed in TBS 3 x 10 min at room temperature and incubated in a
731 solution containing 3% (wt/vol) BSA, 0.25% (vol/vol) Triton X-100, and 4 µg/mL streptavidin
732 conjugated with Alex Fluor 488 (Fisher Scientific) in TBS overnight at 4°C. Slices were washed
733 in TBS 3 x 10 min at room temperature and incubated with 1 µg/mL 4',6-diamidino-2-
734 phenylindole (DAPI) in TBS for two hours at room temperature. Slices were washed in TBS 3 x
735 10 min at room temperature and mounted onto microscope slides and coverslipped using an
736 aqueous mounting medium.
737 Processed slices were imaged using an Olympus Fluoview FV1200 laser-scanning

confocal system connected with an inverted Olympus IX83 microscope and controlled using Olympus Fluoview software (FV10-ASW version 4.0; Olympus). A helium neon laser tuned to 405 nm (DAPI), 488 nm (retrograde labelled neuron), or 543 nm (RetroBeads) and an Olympus UPlanSApo 30X, 1.05 NA silicone oil-immersion objective were used to acquire three-channel image stacks which, when stitched together in three dimensions, contained entire retrograde labelled neurons.

Statistical Analysis

Electrophysiological recordings were analyzed using Clampfit software and custom scripts written for MATLAB software. Statistical analyses were conducted using GraphPad Prism software (version 9, GraphPad Software, Boston, Massachusetts, USA). Data were analysed using the Chi-square test, two-way ANOVA with the Bonferroni *post hoc* correction, or Pearson correlation, as indicated. Data are presented for individual neurons and as group means ± 1 SEM. For all figures, statistical significance is indicated as $*p < 0.05$, $**p < 0.01$, $***\ p < 0.001$, and $****p < 0.0001$. The sample size for each group is listed in the respective figure legend.

Data Availability

All data that were generated and presented in this manuscript are available from the corresponding author (C.D.C.B.) upon reasonable request. Neuron reconstructions from this study will be submitted to NeuroMorpho.org.

References

1 Parikh, V., Kozak, R., Martinez, V. & Sarter, M. Prefrontal acetylcholine release controls cue detection on multiple timescales. *Neuron* **56**, 141-154 (2007).

2 Parikh, V. & Sarter, M. Cholinergic mediation of attention: contributions of phasic and tonic increases in prefrontal cholinergic activity. *Ann.N.Y.Acad.Sci.* **1129**, 225-235 (2008).

3 Guillem, K. *et al.* Nicotinic acetylcholine receptor beta2 subunits in the medial prefrontal cortex control attention. *Science* **333**, 888-891 (2011). https://doi.org:10.1126/science.1207079

4 Disney, A. A. & Higley, M. J. Diverse Spatiotemporal Scales of Cholinergic Signaling in the Neocortex. *The Journal of neuroscience : the official journal of the Society for Neuroscience* **40**, 720-725 (2020). https://doi.org:10.1523/JNEUROSCI.1306-19.2019

5 Sarter, M. & Lustig, C. Forebrain Cholinergic Signaling: Wired and Phasic, Not Tonic, and Causing Behavior. *The Journal of neuroscience : the official journal of the Society for Neuroscience* **40**, 712-719 (2020). https://doi.org:10.1523/JNEUROSCI.1305-19.2019

6 Passetti, F., Dalley, J. W., O'Connell, M. T., Everitt, B. J. & Robbins, T. W. Increased acetylcholine release in the rat medial prefrontal cortex during performance of a visual attentional task. *Eur.J.Neurosci.* **12**, 3051-3058 (2000).

7 Dalley, J. W. *et al.* Distinct changes in cortical acetylcholine and noradrenaline efflux during contingent and noncontingent performance of a visual attentional task. *The Journal of neuroscience : the official journal of the Society for Neuroscience* **21**, 4908-4914 (2001). https://doi.org:10.1523/JNEUROSCI.21-13-04908.2001

8 Bailey, C. D., De Biasi, M., Fletcher, P. J. & Lambe, E. K. The nicotinic acetylcholine receptor alpha5 subunit plays a key role in attention circuitry and accuracy. *The Journal of neuroscience : the official journal of the Society for Neuroscience* **30**, 9241-9252 (2010). https://doi.org:10.1523/JNEUROSCI.2258-10.2010

9 Hoyle, E., Genn, R. F., Fernandes, C. & Stolerman, I. P. Impaired performance of alpha7 nicotinic receptor knockout mice in the five-choice serial reaction time task. *Psychopharmacology (Berl)* **189**, 211-223 (2006).

10 Rezvani, A. H., Bushnell, P. J. & Levin, E. D. Effects of nicotine and mecamylamine on choice accuracy in an operant visual signal detection task in female rats. *Psychopharmacology (Berl)* **164**, 369-375 (2002). https://doi.org:10.1007/s00213-002-1221-0

11 Sabec, M. H., Wonnacott, S., Warburton, E. C. & Bashir, Z. I. Nicotinic Acetylcholine Receptors Control Encoding and Retrieval of Associative Recognition Memory through Plasticity in the Medial Prefrontal Cortex. *Cell Rep* **22**, 3409-3415 (2018). https://doi.org:10.1016/j.celrep.2018.03.016

12 Yang, Y. *et al.* Nicotinic alpha7 receptors enhance NMDA cognitive circuits in dorsolateral prefrontal cortex. *Proceedings of the National Academy of Sciences of the United States of America* **110**, 12078-12083 (2013). https://doi.org:10.1073/pnas.1307849110

13 Castner, S. A. *et al.* Immediate and sustained improvements in working memory after selective stimulation of alpha7 nicotinic acetylcholine receptors. *Biological psychiatry* **69**, 12-18 (2011). https://doi.org:10.1016/j.biopsych.2010.08.006

14 Esaki, H. *et al.* Varenicline enhances recognition memory via alpha7 nicotinic acetylcholine receptors in the medial prefrontal cortex in male mice. *Neuropharmacology* **239**, 109672 (2023). https://doi.org:10.1016/j.neuropharm.2023.109672

15 Abbondanza, A., Urushadze, A., Alves-Barboza, A. R. & Janickova, H. Expression and function of nicotinic acetylcholine receptors in specific neuronal populations: Focus on striatal and prefrontal circuits. *Pharmacol Res* **204**, 107190 (2024). https://doi.org:10.1016/j.phrs.2024.107190

16 Poorthuis, R. B. *et al.* Layer-specific modulation of the prefrontal cortex by nicotinic acetylcholine receptors. *Cereb Cortex* **23**, 148-161 (2013). https://doi.org:10.1093/cercor/bhr390

17 Aracri, P., Meneghini, S., Coatti, A., Amadeo, A. & Becchetti, A. alpha4beta2(*) nicotinic receptors stimulate GABA release onto fast-spiking cells in layer V of mouse prefrontal (Fr2) cortex. *Neuroscience* **340**, 48-61 (2017). https://doi.org:10.1016/j.neuroscience.2016.10.045

18 Zolles, G., Wagner, E., Lampert, A. & Sutor, B. Functional expression of nicotinic acetylcholine receptors in rat neocortical layer 5 pyramidal cells. *Cereb Cortex* **19**, 1079-1091 (2009). https://doi.org:10.1093/cercor/bhn158

19 Agmon, A. & Connors, B. W. Correlation between intrinsic firing patterns and thalamocortical synaptic responses of neurons in mouse barrel cortex. *The Journal of neuroscience : the official journal of the Society for Neuroscience* **12**, 319-329 (1992). https://doi.org:10.1523/JNEUROSCI.12-01-00319.1992

20 Chagnac-Amitai, Y., Luhmann, H. J. & Prince, D. A. Burst generating and regular spiking layer 5 pyramidal neurons of rat neocortex have different morphological features. *The Journal of comparative neurology* **296**, 598-613 (1990). https://doi.org:10.1002/cne.902960407

21 Chang, Y. M. & Luebke, J. I. Electrophysiological diversity of layer 5 pyramidal cells in the prefrontal cortex of the rhesus monkey: in vitro slice studies. *Journal of neurophysiology* **98**, 2622-2632 (2007). https://doi.org:10.1152/jn.00585.2007

22 Chen, W., Zhang, J. J., Hu, G. Y. & Wu, C. P. Electrophysiological and morphological properties of pyramidal and nonpyramidal neurons in the cat motor cortex in vitro. *Neuroscience* **73**, 39-55 (1996). https://doi.org:10.1016/0306-4522(96)00009-7

23 Franceschetti, S., Sancini, G., Panzica, F., Radici, C. & Avanzini, G. Postnatal differentiation of firing properties and morphological characteristics in layer V pyramidal neurons of the sensorimotor cortex. *Neuroscience* **83**, 1013-1024 (1998). https://doi.org:10.1016/s0306-4522(97)00463-6

24 Groh, A. *et al.* Cell-type specific properties of pyramidal neurons in neocortex underlying a layout that is modifiable depending on the cortical area. *Cereb Cortex* **20**, 826-836 (2010). https://doi.org:10.1093/cercor/bhp152

25 Kim, E. J., Juavinett, A. L., Kyubwa, E. M., Jacobs, M. W. & Callaway, E. M. Three Types of Cortical Layer 5 Neurons That Differ in Brain-wide Connectivity

and Function. *Neuron* **88**, 1253-1267 (2015). https://doi.org:10.1016/j.neuron.2015.11.002

26 McCormick, D. A., Connors, B. W., Lighthall, J. W. & Prince, D. A. Comparative electrophysiology of pyramidal and sparsely spiny stellate neurons of the neocortex. *Journal of neurophysiology* **54**, 782-806 (1985). https://doi.org:10.1152/jn.1985.54.4.782

27 Otsuka, T. & Kawaguchi, Y. Firing-pattern-dependent specificity of cortical excitatory feed-forward subnetworks. *The Journal of neuroscience : the official journal of the Society for Neuroscience* **28**, 11186-11195 (2008). https://doi.org:10.1523/JNEUROSCI.1921-08.2008

28 Otsuka, T. & Kawaguchi, Y. Cell diversity and connection specificity between callosal projection neurons in the frontal cortex. *The Journal of neuroscience : the official journal of the Society for Neuroscience* **31**, 3862-3870 (2011). https://doi.org:10.1523/JNEUROSCI.5795-10.2011

29 Schubert, D., Kotter, R., Luhmann, H. J. & Staiger, J. F. Morphology, electrophysiology and functional input connectivity of pyramidal neurons characterizes a genuine layer va in the primary somatosensory cortex. *Cereb Cortex* **16**, 223-236 (2006). https://doi.org:10.1093/cercor/bhi100

30 Schubert, D. *et al.* Layer-specific intracolumnar and transcolumnar functional connectivity of layer V pyramidal cells in rat barrel cortex. *The Journal of neuroscience : the official journal of the Society for Neuroscience* **21**, 3580-3592 (2001). https://doi.org:10.1523/JNEUROSCI.21-10-03580.2001

31 van Aerde, K. I. & Feldmeyer, D. Morphological and physiological characterization of pyramidal neuron subtypes in rat medial prefrontal cortex. *Cereb Cortex* **25**, 788-805 (2015). https://doi.org:10.1093/cercor/bht278

32 Yang, C. R., Seamans, J. K. & Gorelova, N. Electrophysiological and morphological properties of layers V-VI principal pyramidal cells in rat prefrontal cortex in vitro. *The Journal of neuroscience : the official journal of the Society for Neuroscience* **16**, 1904-1921 (1996). https://doi.org:10.1523/JNEUROSCI.16-05-01904.1996

33 Mason, A. & Larkman, A. Correlations between morphology and electrophysiology of pyramidal neurons in slices of rat visual cortex. II. Electrophysiology. *The Journal of neuroscience : the official journal of the Society for Neuroscience* **10**, 1415-1428 (1990). https://doi.org:10.1523/JNEUROSCI.10-05-01415.1990

34 Wang, Y. *et al.* Heterogeneity in the pyramidal network of the medial prefrontal cortex. *Nat Neurosci* **9**, 534-542 (2006). https://doi.org:10.1038/nn1670

35 Brown, S. P. & Hestrin, S. Intracortical circuits of pyramidal neurons reflect their long-range axonal targets. *Nature* **457**, 1133-1136 (2009). https://doi.org:10.1038/nature07658

36 Hattox, A. M. & Nelson, S. B. Layer V neurons in mouse cortex projecting to different targets have distinct physiological properties. *Journal of neurophysiology* **98**, 3330-3340 (2007). https://doi.org:10.1152/jn.00397.2007

37 Joshi, A. *et al.* Cell-specific activity-dependent fractionation of layer 2/3-->5B excitatory signaling in mouse auditory cortex. *The Journal of neuroscience : the*

894 *official journal of the Society for Neuroscience* **35**, 3112-3123 (2015).
895 https://doi.org:10.1523/JNEUROSCI.0836-14.2015
896 38 Kalmbach, B. E. *et al.* Signature morpho-electric, transcriptomic, and dendritic
897 properties of human layer 5 neocortical pyramidal neurons. *Neuron* **109**, 2914-
898 2927 e2915 (2021). https://doi.org:10.1016/j.neuron.2021.08.030
899 39 Takahashi, N. *et al.* Active dendritic currents gate descending cortical outputs in
900 perception. *Nat Neurosci* **23**, 1277-1285 (2020). https://doi.org:10.1038/s41593-
901 020-0677-8
902 40 Hallman, L. E., Schofield, B. R. & Lin, C. S. Dendritic morphology and axon
903 collaterals of corticotectal, corticopontine, and callosal neurons in layer V of
904 primary visual cortex of the hooded rat. *The Journal of comparative neurology*
905 **272**, 149-160 (1988). https://doi.org:10.1002/cne.902720111
906 41 Gao, W. J. & Zheng, Z. H. Target-specific differences in somatodendritic
907 morphology of layer V pyramidal neurons in rat motor cortex. *The Journal of*
908 *comparative neurology* **476**, 174-185 (2004). https://doi.org:10.1002/cne.20224
909 42 Zhang, Y. *et al.* Pinpointing Morphology and Projection of Excitatory Neurons in
910 Mouse Visual Cortex. *Front Neurosci* **13**, 912 (2019).
911 https://doi.org:10.3389/fnins.2019.00912
912 43 Jiang, S. *et al.* Anatomically revealed morphological patterns of pyramidal
913 neurons in layer 5 of the motor cortex. *Sci Rep* **10**, 7916 (2020).
914 https://doi.org:10.1038/s41598-020-64665-2
915 44 Avesar, D. & Gulledge, A. T. Selective serotonergic excitation of callosal
916 projection neurons. *Front Neural Circuits* **6**, 12 (2012).
917 https://doi.org:10.3389/fncir.2012.00012
918 45 Dembrow, N. C., Chitwood, R. A. & Johnston, D. Projection-specific
919 neuromodulation of medial prefrontal cortex neurons. *The Journal of*
920 *neuroscience : the official journal of the Society for Neuroscience* **30**, 16922-
921 16937 (2010). https://doi.org:10.1523/JNEUROSCI.3644-10.2010
922 46 Wu, J. *et al.* Heteromeric alpha7beta2 Nicotinic Acetylcholine Receptors in the
923 Brain. *Trends Pharmacol Sci* **37**, 562-574 (2016).
924 https://doi.org:10.1016/j.tips.2016.03.005
925 47 Murray, T. A. *et al.* alpha7beta2 nicotinic acetylcholine receptors assemble,
926 function, and are activated primarily via their alpha7-alpha7 interfaces. *Molecular*
927 *pharmacology* **81**, 175-188 (2012). https://doi.org:10.1124/mol.111.074088
928 48 Thomsen, M. S. *et al.* alpha7 and beta2 Nicotinic Acetylcholine Receptor
929 Subunits Form Heteromeric Receptor Complexes that Are Expressed in the
930 Human Cortex and Display Distinct Pharmacological Properties. *PloS one* **10**,
931 e0130572 (2015). https://doi.org:10.1371/journal.pone.0130572
932 49 Chung, B. Y. T. & Bailey, C. D. C. Similar nicotinic excitability responses across
933 the developing hippocampal formation are regulated by small-conductance
934 calcium-activated potassium channels. *Journal of neurophysiology* **119**, 1707-
935 1722 (2018). https://doi.org:10.1152/jn.00426.2017
936 50 Hay, Y. A., Lambolez, B. & Tricoire, L. Nicotinic Transmission onto Layer 6
937 Cortical Neurons Relies on Synaptic Activation of Non-alpha7 Receptors. *Cereb*
938 *Cortex* **26**, 2549-2562 (2016). https://doi.org:10.1093/cercor/bhv085

939 51 Kroon, T., van Hugte, E., van Linge, L., Mansvelder, H. D. & Meredith, R. M.
940 Early postnatal development of pyramidal neurons across layers of the mouse
941 medial prefrontal cortex. *Sci Rep* **9**, 5037 (2019). https://doi.org:10.1038/s41598-
942 019-41661-9
943 52 Patel, A. V. *et al.* Developmental age and biological sex influence muscarinic
944 receptor function and neuron morphology within layer VI of the medial prefrontal
945 cortex. *Cereb Cortex* **32**, 3137-3158 (2022).
946 https://doi.org:10.1093/cercor/bhab406
947 53 Bailey, C. D., Alves, N. C., Nashmi, R., De Biasi, M. & Lambe, E. K. Nicotinic
948 alpha5 subunits drive developmental changes in the activation and morphology
949 of prefrontal cortex layer VI neurons. *Biological psychiatry* **71**, 120-128 (2012).
950 https://doi.org:10.1016/j.biopsych.2011.09.011
951 54 Hoover, W. B. & Vertes, R. P. Anatomical analysis of afferent projections to the
952 medial prefrontal cortex in the rat. *Brain Struct Funct* **212**, 149-179 (2007).
953 https://doi.org:10.1007/s00429-007-0150-4
954 55 Gabbott, P. L., Warner, T. A., Jays, P. R., Salway, P. & Busby, S. J. Prefrontal
955 cortex in the rat: projections to subcortical autonomic, motor, and limbic centers.
956 *J.Comp Neurol.* **492**, 145-177 (2005).
957 56 Verhoog, M. B. *et al.* Layer-specific cholinergic control of human and mouse
958 cortical synaptic plasticity. *Nat Commun* **7**, 12826 (2016).
959 https://doi.org:10.1038/ncomms12826
960 57 Komal, P., Gudavicius, G., Nelson, C. J. & Nashmi, R. T-cell receptor activation
961 decreases excitability of cortical interneurons by inhibiting alpha7 nicotinic
962 receptors. *The Journal of neuroscience : the official journal of the Society for*
963 *Neuroscience* **34**, 22-35 (2014). https://doi.org:10.1523/JNEUROSCI.2093-
964 13.2014
965 58 Obermayer, J. *et al.* Prefrontal cortical ChAT-VIP interneurons provide local
966 excitation by cholinergic synaptic transmission and control attention. *Nat*
967 *Commun* **10**, 5280 (2019). https://doi.org:10.1038/s41467-019-13244-9
968 59 Lambe, E. K., Picciotto, M. R. & Aghajanian, G. K. Nicotine induces glutamate
969 release from thalamocortical terminals in prefrontal cortex.
970 *Neuropsychopharmacology* **28**, 216-225 (2003).
971 https://doi.org:10.1038/sj.npp.1300032
972 60 Alves, N. C., Bailey, C. D., Nashmi, R. & Lambe, E. K. Developmental sex
973 differences in nicotinic currents of prefrontal layer VI neurons in mice and rats.
974 *PLoS.One.* **5**, e9261 (2010).
975 61 Hedrick, T. & Waters, J. Spiking patterns of neocortical L5 pyramidal neurons in
976 vitro change with temperature. *Front Cell Neurosci* **5**, 1 (2011).
977 https://doi.org:10.3389/fncel.2011.00001
978 62 Joshi, A., Kalappa, B. I., Anderson, C. T. & Tzounopoulos, T. Cell-Specific
979 Cholinergic Modulation of Excitability of Layer 5B Principal Neurons in Mouse
980 Auditory Cortex. *The Journal of neuroscience : the official journal of the Society*
981 *for Neuroscience* **36**, 8487-8499 (2016).
982 https://doi.org:10.1523/JNEUROSCI.0780-16.2016

63 Gao, L. *et al.* Single-neuron analysis of dendrites and axons reveals the network organization in mouse prefrontal cortex. *Nat Neurosci* **26**, 1111-1126 (2023). https://doi.org:10.1038/s41593-023-01339-y

64 Works, S. J., Wilson, R. E. & Wellman, C. L. Age-dependent effect of cholinergic lesion on dendritic morphology in rat frontal cortex. *Neurobiology of aging* **25**, 963-974 (2004). https://doi.org:10.1016/j.neurobiolaging.2003.08.003

65 Vertes, R. P. Differential projections of the infralimbic and prelimbic cortex in the rat. *Synapse* **51**, 32-58 (2004).

66 Ding, D. C., Gabbott, P. L. & Totterdell, S. Differences in the laminar origin of projections from the medial prefrontal cortex to the nucleus accumbens shell and core regions in the rat. *Brain research* **917**, 81-89 (2001). https://doi.org:10.1016/s0006-8993(01)02912-2

67 Musall, S. *et al.* Pyramidal cell types drive functionally distinct cortical activity patterns during decision-making. *Nat Neurosci* **26**, 495-505 (2023). https://doi.org:10.1038/s41593-022-01245-9

68 Mohan, H. *et al.* Cortical glutamatergic projection neuron types contribute to distinct functional subnetworks. *Nat Neurosci* **26**, 481-494 (2023). https://doi.org:10.1038/s41593-022-01244-w

69 Nakayama, H., Ibanez-Tallon, I. & Heintz, N. Cell-Type-Specific Contributions of Medial Prefrontal Neurons to Flexible Behaviors. *The Journal of neuroscience : the official journal of the Society for Neuroscience* **38**, 4490-4504 (2018). https://doi.org:10.1523/JNEUROSCI.3537-17.2018

70 de Kloet, S. F. *et al.* Bi-directional regulation of cognitive control by distinct prefrontal cortical output neurons to thalamus and striatum. *Nat Commun* **12**, 1994 (2021). https://doi.org:10.1038/s41467-021-22260-7

71 Womelsdorf, T., Ardid, S., Everling, S. & Valiante, T. A. Burst firing synchronizes prefrontal and anterior cingulate cortex during attentional control. *Curr Biol* **24**, 2613-2621 (2014). https://doi.org:10.1016/j.cub.2014.09.046

72 Voloh, B. & Womelsdorf, T. Cell-Type Specific Burst Firing Interacts with Theta and Beta Activity in Prefrontal Cortex During Attention States. *Cereb Cortex* **28**, 4348-4364 (2018). https://doi.org:10.1093/cercor/bhx287

73 Papke, R. L. & Lindstrom, J. M. Nicotinic acetylcholine receptors: Conventional and unconventional ligands and signaling. *Neuropharmacology* **168**, 108021 (2020). https://doi.org:10.1016/j.neuropharm.2020.108021

74 Paxinos, G. & Franklin, K. B. J. *The mouse brain in stereotaxic coordinates*. 2nd edn, (Academic, 2001).

75 Myatt, D. R., Hadlington, T., Ascoli, G. A. & Nasuto, S. J. Neuromantic - from semi-manual to semi-automatic reconstruction of neuron morphology. *Front Neuroinform* **6**, 4 (2012). https://doi.org:10.3389/fninf.2012.00004

Acknowledgements

Funding for this work was provided by Discovery Grants from the Natural Sciences and Engineering Council of Canada (NSERC) to C.D.C.B. (RGPIN-2019-04989) and E.C. (RGPIN-2018-04699), and by a Canada Foundation for Innovation (CFI) grant to C.D.C.B. (30381). We thank Dr. Matthew Vickaryous at the University of Guelph for the use of a fluorescence filter cube.

Author contributions

A.V.P. and C.D.C.B. conceived and designed the study. A.V.P., A.N., and P.P. performed experiments. E.C. provided resources and supervised experiments. C.D.C.B. supervised the entire study. A.V.P. and C.D.C.B. analyzed all results and wrote the manuscript. All authors have reviewed and approved the final manuscript.

Competing interests

The authors declare no competing interests.